A Comprehensive Assessment of a new series of 5',6'-difluorobenzotriazole-acrylonitrile derivatives as Microtubule Targeting Agents (MTAs)

Federico Riu [a], Luca Sanna [b], Roberta Ibba [a,*], Sandra Piras [a], Valentina Bordoni [b], M. Andrea Scorciapino [c], Michele Lai [d,e], Simona Sestito [a], Luigi Bagella [b,f,*], Antonio Carta [a]

[a] *Department of Chemistry and Pharmacy, University of Sassari, via Vienna 2, 07100, Sassari, Italy.*
[b] *Department of Biomedical Sciences, University of Sassari, viale San Pietro 43/b, 07100, Sassari, Italy.*
[c] *Department of Chemical and Geological Sciences, University of Cagliari, S.P. 8 km 0.700, 09042, Monserrato (CA), Italy.*
[d] *Retrovirus Centre, Department of Translational Medicine and New Technologies in Medicine and Surgery, University of Pisa, Strada Statale del Brennero, 2, Pisa, Italy.*
[e] *CISUP - Centre for Instrumentation Sharing - University of Pisa, Lungarno Pacinotti 43, Pisa.*
[f] *Sbarro Institute for Cancer Research and Molecular Medicine, Center for Biotechnology, College of Science and Technology, Temple University, Philadelphia, PA, 19122, USA.*
* *Corresponding authors. Email addresses: ribba@uniss.it (R. Ibba), lbagella@uniss.it (L. Bagella)*

Abstract

Microtubules (MTs) are the principal target for drugs acting against mitosis. These compounds, called microtubule targeting agents (MTAs), cause a mitotic arrest during G2/M phase, subsequently inducing cell apoptosis. MTAs could be classified in two groups: microtubule stabilising agents (MSAs) and microtubule destabilising agents (MDAs). In this paper we present a new series of (*E*)(*Z*)-2-(5,6-difluoro-(1*H*)2*H*-benzo[*d*][1,2,3]triazol-1(2)-yl)-3-(*R*)acrylonitrile (**9a-j**, **10e**, **11a**,**b**) and (*E*)-2-(1*H*-benzo[*d*][1,2,3]triazol-1-yl)-3-(*R*)acrylonitrile derivatives (**13d**,**j**), which were recognised to act as MTAs agents. They were rationally designed, synthesised, characterised and subjected to different biological assessments. Computational docking was carried out in order to investigate the potential binding to the colchicine-binding site on tubulin. From this first prediction, the di-fluoro substitution seemed to be beneficial for the binding affinity with tubulin. The new fluorine derivatives, here presented, showed an improved antiproliferative activity when compared to the previously reported compounds. The biological evaluation included a preliminary antiproliferative screening on NCI60 cancer cells panel (1-10 μM). Compound **9a** was selected as lead compound of the new series of derivatives. The *in vitro* XTT assay, flow cytometry analysis and immunostaining performed on HeLa cells treated with **9a** showed a considerable antiproliferative effect, (IC50 = 3.2 μM), an increased number of cells in G2/M-phase, followed by an enhancement in ell division defects. Moreover, β-tubulin staining confirmed **9a** as a MDA triggering tubulin disassembly. Then, the co-administration of compound **9a** and an extrusion pump inhibitor (EPI) was investigated: the association resulted beneficial for the antiproliferative activity and compound **9a** showed to be client of extrusion pumps. Finally, structural superimposition of different colchicine binding site inhibitors (CBIs) in clinical trial and our MDA, provided an additional confirmation of the targeting to the predicted binding site. Physicochemical, pharmacokinetic and druglikeness predictions were also conducted and all the newly synthesised derivatives showed to be drug-like molecules.

Keywords: microtubule targeting agents; benzotriazoles; tubulin; extrusion pump inhibition; cell growth inhibition; molecular docking.

1. Introduction

Cancer is one of the noncommunicable diseases (NCDs) and it is expected to become the leading death cause and the principal obstacle for the increase of life expectancy in the 21st century. [1] Deaths caused by cancer represent approximately 22% of all NCD casualties. [2] The actual shortage of efficient and safe drugs for cancer treatment is a driving force for research efforts in this field. [3] One of the main feature of a tumour cell is its uncontrolled division. Cell division cycle consists of four successive phases called G1 (Gap 1), S (DNA synthesis), G2 (Gap 2), and M (mitosis). Cell cycle phases convey important information regarding the cytotoxic potential of anticancer drugs. [4] A crucial element involved during cell replication is the mitotic spindle, mainly composed by microtubules (MTs), which are filaments consisting in α- and β-tubulin heterodimers. An attractive approach pursued for the development of new therapeutic agents for cancer treatment is the interference with the MT dynamic equilibrium. [5–7] A wide variety of compounds targeting mitotic spindle have been designed and investigated. [8] However, little is known about the mechanism of cell death triggered by those drugs. Generally, drugs acting against cell division cycle lead to mitotic arrest during G2/M phase, subsequently inducing cell apoptosis. Nowadays, microtubule targeting agents (MTAs) are some of the most effective drugs used in the treatment of both solid and haematological tumours. [9] MTAs could be classified in two groups on the basis of their mechanism of action: microtubule stabilising agents (MSAs) and microtubule destabilising agents (MDAs). Both types of agents showed to suppress cellular microtubule dynamics. [10] MTAs could also be categorised into 5 classes based on their interactions with the taxane-, vinca-, colchicine-, laulimalide/peloruside-, pironetin- or the maytansine-binding site on tubulin. [11] Colchicine binding site inhibitors (CBSIs), comprise a variety of small molecules which include colchicine and combretastatins A-1 (CA-1) and A-4 (CA-4), which bind in the colchicine site (CBS) located on β-tubulin at its interface with α-tubulin. [12,13] Although some CBISs, such as combretastatin A-4 phosphate (CA-4P) and A-1 diphosphate (CA-1P), 2-methoxyestradiol and verubulin have been evaluated in phase 1 and 2 clinical trials, [14] no CBIS compound has been approved as anticancer agent so far. Hence, this binding site provides new challenging opportunities for drug discovery. [15–17] We already published a group of benzotriazolacrylonitrile derivatives which turned out to act as CBSIs. [18–23] All derivatives can be grouped into two different chemical classes: 1*H*-benzotriazole derivatives which showed good activity, and the parental 2*H*-benzotriazole derivatives with a weaker antiproliferative activity. [18] Among all synthesised derivatives, (*E*)-2-(1*H*-benzo[*d*][1,2,3]triazol-1-yl)-3-(4-methoxyphenyl)acrylonitrile was identified as lead compound, hereinafter and in literature [19] labelled as compound **34**. Cell cycle analysis on K-562 cells (leukemia) revealed that compound **34** inhibits the G2/M phase of cell cycle, [21] with an IC_{50} value of 0.2 μM on CCRF-CCM leukemia cells. [19] Overall, our experimental and computational investigations supported the hypothesis that these compounds act as antiproliferative agents by interacting with tubulin in the colchicine-binding site. Therefore, compound **34** could be classified as MDAs, since it inhibits the tubulin assembly. [21] The novelty of the present work is based on the introduction of fluorine atoms into the benzotriazole moiety. The replacement of hydrogens with fluorine atoms is a widely used approach in medicinal chemistry to improve relevant drug-like properties such as metabolic stability, bioavailability and ligand-protein interactions (by altering the pK_a). [24] As a matter of fact, aromatic fluorination can also increase the compound lipophilicity, [25] and could be used to protect some metabolically weak sites easily affected by Cytochrome P450-dependent oxidation. [26] On this basis, our project aimed to design and synthesise new optimised benzotriazole-acrylonitrile derivatives suitably functionalised with two small halogen atoms, such as fluorine, in position 5' and 6' on the benzotriazole moiety as depicted in Figure 1. Therefore, in this paper we present a new series

of (*E*)(*Z*)-2-(5,6-difluoro-(1*H*)2*H*-benzo[*d*][1,2,3]triazol-1(2)-yl)-3-(*R*)acrylonitrile (**9a-j**, **10e**, **11a**,**b**) and (*E*)-2-(1*H*-benzo[*d*][1,2,3]triazol-1-yl)-3-(*R*)acrylonitrile derivatives (**13d**,**j**), which were rationally designed, synthesised, characterised and submitted to different biological assessments.

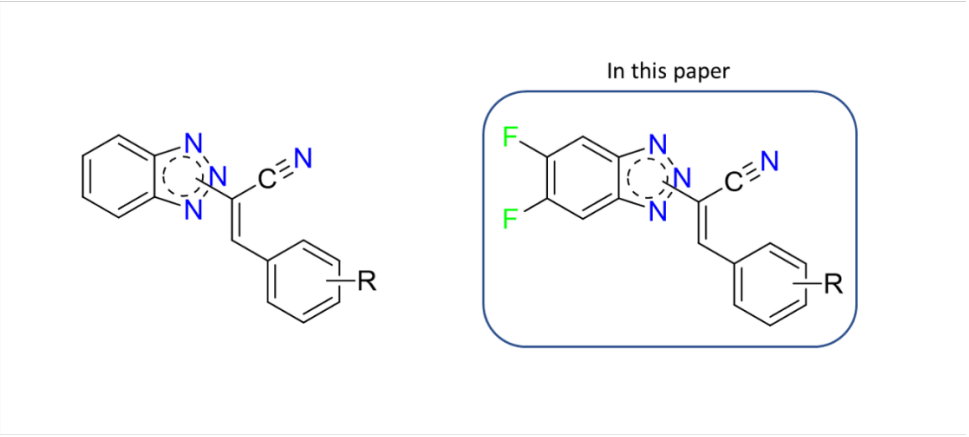

Figure 1. General structure of previously reported compounds (left) and newly designed di-fluoro benzotriazole-acrylonitrile derivatives (right).

2. Material and Methods

2.1. Molecular Docking

AutoDock Vina 1.1.2. [27] version 1.5.6 was selected for its known sampling and scoring functions. [28] Tubulin-Colchicine complex (PDB code: 4O2B; resolution: 2.30 Å) structure was provided by the Protein Data Bank (rcsb.org). [29] Protein structures have been employed removing H_2O molecules, MES (buffer, 2-(*N*-morpholino)-ethanesulfonic acid), GOL (glycerol), ions (Ca^{2+}, Mg^{2+}), GTP (Guanosine-5'-triphosphate), GDP (Guanosine-5'-diphosphate), but also chains C, D, E, F, in order to analyse the docking poses of ligands in a free binding pocket. The structures were visualised and analysed in PyMOL 2.3.4. AutoDockTools (ADT) [30] was used to obtain not only the PDBQT files of both protein structures and all ligands, but also to determine the docking Grid Box (30-30-30 Å for x,y,z coordinates). Docking was performed using the protein in its rigid form, or by making some amino acids flexible: Serα178, Thrα179, Alaα180, Alaα181. These amino acids are known to establish important H-bonds with the colchicine-binding pocket of tubulin. The exhaustiveness value was set to 8 and the number of poses to 10 for each Vina docking calculation. The binding energy range was imposed to be ≤ 2 kcal/mol above that of the best binding pose for each ligand. 2D-pictures of the binding interactions between ligands and the protein binding pocket were made with two molecular- graphics programs: LigPlot$^+$ v.2.2. and Maestro (Schrödinger package). LigPlot$^+$ processed in 2D-dimension the protein-ligand interaction with a cutoff of 5 Å from the centre of the ligand. Maestro's Ligand Interaction Diagram is a 2D binding site representation known for the accuracy in the placement of residues. Structural superimposition of the docked pose of compound **9a** and the crystal structure of tubulin co-crystallised with colchicine, as well as other CBSIs, were represented with PyMOL. The crystallized structures of tubulin/ligand complexes were obtained from the Protein Data Bank: colchicine (PDB code: 4O2B), tivantinib (TIV, PDB code: 5CB4), plinabulin (PLI, PDB code: 5C8Y), crolibulin (CRO, PDB code: 6JCJ).The docking calculations were

conducted on a PC with an Intel® Core™ i7-9705H CPU @ 2.60 GHz with 8 GB RAM (operating system: Ubuntu 16.04, 6 CPUs for each calculation).

2.2. Chemistry

2.2.1. Materials

3,4-difluoroaniline (**1**) and the aldehydes (**8a–j**) were commercially available.

2.2.2. Synthetic Methods

The synthesis, as depicted in Scheme 1, starts with the commercially available 3,4-difluoroaniline (**1**), which was in the first place acetylated with acetic anhydride, gaining compound **2**. The following nitration of the amidic compound **2** with a solution of KNO_3 in H_2SO_{4conc} (concentrated H_2SO_4), resulted in the formation of nitro-derivative **3**. Then, 4,5-difluoro-2-nitroaniline **4** was obtained by hydrolytic deprotection with H_2SO_{4conc}. The reduction of nitro group brought to 4,5-difluorobenzene-1,2-diamine (**5**). The dianiline derivative **5** is cyclised with $NaNO_2$ in HCl, obtaining 5',6'-difluorobenzotriazole (**6**). Reaction of **6** with chloroacetonitrile ($ClCH_2CN$) was performed, in the presence of KOH in acetonitrile, to obtain two geometric isomers bearing an acetonitrile chain on the triazole ring **7a**,**b**. The final step corresponds to a Knoevenagel condensation between each acetonitrile isomer (**7a**,**b**), separately, and the appropriate, commercially purchased, aldehydes (**8a-j**), bringing to final (*E*)(*Z*)-2-(5,6-difluoro-(1*H*)2*H*-benzo[*d*][1,2,3]triazol-1(2)-yl)-3-(*R*)acrylonitrile derivatives **9a-j**, **10e**, and **11a**,**b**. The final step generally brings to the sole formation of the *E*-isomer, only in one case a *Z*-isomer compound was identified and purified from the reaction mixture. A Knoevenagel condensation between 2-(1*H*-benzo[*d*][1,2,3]triazol-1-yl)acetonitrile **12a** and aldehydes **8d**,**j** gave final compounds **13d**,**j**. Compounds were purified by flash chromatography or by crystallisation from ethanol. For flash chromatography, Merck silica gel 60 was used with a particle size of 0.040-0.063mm (230-400 mesh ASTM), and a proper eluent mixture of petroleum spirit (PS), diethyl ether (DE), ethyl acetate (EA), chloroform ($CHCl_3$) and methanol (CH_3OH).

2.2.3. Chemical characterisation

Evaporation was performed *in vacuo* (rotating evaporator). Sodium sulfate was always used as the drying agent. Celite® 545 was used as filter agent. Commercially available chemicals were purchased from Sigma Aldrich and Carlo Erba Reagents. Retention factors (R_f) were obtained using a mixture of petroleum spirit (PS) and ethyl acetate (EA) as eluents (8/2 respectively), to develop Thin Layer Chromatographies (TLCs), Merck F-254 plates were used. Melting points (m.p.) of the compounds were measured in a Köfler hot stage in open capillaries or Digital Electrothermal melting point apparatus and are uncorrected. The compounds were dissolved in CH_3CN for HPLC (concentration of 1.0-2.0 ppm) for ESI-MS characterisation. Mass spectra (full mass) were obtained on a Q Exactive Plus Hybrid Quadrupole-Orbitrap mass spectrometer of Thermo Fisher Scientific, in the positive-ion and negative-ion mode. The solutions were infused at a flow rate of 5.00 μL/min into the ESI chamber. The spectra were recorded in the *m/z* range 150–800 at a resolution of 140 000 and accumulated for at least 2 min in order to increase the signal-to-noise ratio. Measurements conditions for positive-ion were as follows: spray voltage 2300 V, capillary temperature 250 °C, sheath gas 10 (arbitrary units), auxiliary gas 3 (arbitrary units), sweep gas 0 (arbitrary units) and probe heater temperature 50 °C. Measurements conditions for negative-ion were as follows: spray voltage −1900 V, capillary temperature 250 °C, sheath gas 20 (arbitrary units), auxiliary gas 5 (arbitrary units),

sweep gas 0 (arbitrary units), probe heater temperature 50 °C. ESI-MS spectra were analysed by using Thermo Xcalibur 3.0.63 software (Thermo Fisher Scientific), and the Xtract tool (integrated into the software) was used to extract the average deconvoluted monoisotopic masses. Nuclear Magnetic Resonance (NMR) spectra were registered in solutions in deuterated DMSO and recorded with a Bruker Avance III 400 NanoBay (400 MHz). ^{1}H-NMR chemical shifts are reported in parts per million (ppm) downfield from tetramethylsilane (TMS) used as internal standard. Chemical shift values are reported in ppm (δ) and coupling constants (J) are reported in Hertz (Hz). The assignment of exchangeable protons (OH and NH) was confirmed by the addition of D_2O. Signal multiplicities are represented as s (singlet), d (doublet), dd (doublet of doublets), ddd (doublet of doublets of doublets), t (triplet), m (multiplet) and wm (wide multiplet). ^{13}C-NMR chemical shifts are reported in downfield from tetramethylsilane (TMS) used as internal standard, jmod (*J*-modulated spin-echo for X-nuclei coupled to H-1 to determine number of attached protons) was selected as most suitable method. For the *E*/*Z*-isomers characterisation (Paragraph 1.1.), ^{1}H-NMR spectra were acquired on an Agilent INOVA-500 spectrometer with an operative Larmor frequency of 500.3 MHz, by using a 6.1 μs pulse (90°), 1 s delay time, 1.5 s acquisition time, 8 transients and a spectral width of 9 kHz. ^{1}H-^{1}H correlation TOCSY experiments were recorded over the same spectral window using 2048 complex points and sampling each of the 256 increments with 8 scans and by applying 80 ms spin-lock with the MLEV-17 mixing scheme. The same acquisition parameters were applied for the acquisition of the NOESY experiments with 200 ms mixing time. In addition, a series of selective DPFGSE (Double Pulse Field Gradient Spin-Echo) one-dimensional NOESY [31] were performed with the same parameters as for standard ^{1}H acquisition with 128 transients and either 250, 500 and 750 ms mixing time. Resonance assignments were obtained on the basis of relative intensity, chemical shift and fine structure, together with results from TOCSY and NOESY 2D spectra as well as the database at www.nmrdb.org. [32]

2.3. Biology

2.3.1. NCI60 testing screen: in vitro antiproliferative assay

The first *in vitro* anti-cancer screening was performed through the NCI60 test, provided by the Developmental Therapeutics Program of the National Cancer Institute (NCI, Bethesda, USA). At the beginning, a single high dose of 10 μM of the compound is tested in the full NCI60 cell panel. If the inhibition results agree with the selection criteria, the same compound can be tested again in 5x10-fold dilutions, from 100 μM up to 0.01 μM. More details about the NCI60 experiments are reported in the Supplementary Material (Table S1 and Figures S34-53) and in the NCI website (https://dtp.cancer.gov).

2.3.2. HeLa cells culture

HeLa cells (human cervix epithelioid carcinoma) (ATCC, Rockville, MD) have been cultured with Dulbecco's Modified Eagle Medium (DMEM) (Gibco). Medium has been supplemented with 10% of Fetal Bovine Serum (FBS), 100 μg/mL streptomycin, 100 units/mL penicillin (Gibco) and 1% of l-glutamine. Cells were incubated at 37 °C in a humidified atmosphere containing 5% of CO_2.

2.3.3. Proliferation Assay on HeLa cells

HeLa cells were seeded at a density of 1500 cells/wells in a 96 wells-plate. After 24 hours from seeding, cells were treated with different concentrations of **9a** in a range between 0.1 μM and 5 μM

for 24 and 48 hours in a final volume of 100 µL. Before using, **9a** has been resuspended in DMSO which has been used as control. After 24 and 48 hours of incubation with **9a**, XTT assay was performed using Cell Proliferation Kit II (Roche, Basel, Switzerland) and following the manufacture's protocol. Specifically, a volume of 100 µL with 74.5 µL of medium, 25 µL of labelling reagent and 0.5 µL of XTT electron coupling was added to each well and then incubated at 37 °C for 4 hours. After incubation, the absorbance was quantified at 490 nm using a spectrophotometric plate reader (SPECTRAMax 384 PLUS). Later on, data obtained were used for the calculation of IC_{50} value using Graphpad Prism software (San Diego, CA, USA). More than three independent experiments were carried out for each treatment and performed in triplicate.

2.3.4. Cell cycle analysis

Based on their phenotype and population doubling, HeLa cells were seeded at 50% of confluence on 6 cm dishes. After 24 hours, cells were treated with a concentration of 5 or 10 µM of **9a**. Later on, adherent and floating cells (dead cells) were initially centrifuged for 5 minutes at 3000 rpm, then washed in PBS and fixed with ice-cold ethanol at 70% in agitation on a vortex to dissolve cluster and permeabilise the membranes. After incubation overnight at -20 °C, fixed HeLa cells were washed twice with cold PBS and finally resuspended in 200 µL of a mix containing PBS and 20 µL/test of 7-AAD (Bioscience, San Diego, CA) and incubated at room temperature for 20 minutes. Flow cytometry was performed for cell cycle analysis using BD FACS CANTO II. For each sample 20000 events were collected and then analysed through BD FACS DIVA software.

2.3.5. Immunostaining

HeLa cells (10^5/well) were seeded 24 hours before treatment with **9a** (0.1 and 0.3 µM). After 48 hours cells were fixed with PFA 4% (paraformaldehyde). Cells were permeabilised via three washes in PBS containing 0.3% Triton X-100 (PBST) and then blocked in PBST containing 1% BSA. Primary antibody β-tubulin (ab179512) was added in blocking solution for 2 hours. Then, 488 anti-rabbit secondary antibody (Alexa Fluor, Thermo Scientific) was incubated for 1 hour. Images were taken using 20x objectives (Evos FL2 Auto, Thermo Scientific). Statistical analysis was performed on 3 biological and technical replicates, using the Kruskal-Wallis test with multiple comparisons.

2.3.6. High-Content Imaging of HeLa Cells and EC_{50} calculation

Imaging experiments were performed using an Operetta CLS high-content imaging device (PerkinElmer, Hamburg, Germany), and analyzed with Harmony 4.6 software (PerkinElmer). To assess the tubulin integrity, we analyzed HeLa cells using 63x magnification, taking 25 fields per sample in biological and technical triplicates. Data were analyzed using the following building blocks: 1- Find Nuclei, 2- Find Cytoplasm (Tubulin+). EC_{50} was obtained by counting the number of nuclei in each field. Cell dimensions were assessed using the following building blocks: 1- Find Nuclei, 2- Find Cytoplasm (Tubulin+), 3- Calculate Morphology properties (Area), as previously described. [33]

*2.3.7. Cytotoxicity evaluation of compound **9a** in presence or absence of extrusion pump inhibitor (EPI)*

Cells were plated in a 384 multiwell plate and treated with **9a** (5 concentrations) in absence or presence (co-treatment) of EPI **SS26**. As negative control, cells were treated with vehicle solution (DMSO 0.3%). All treatments were performed at 0.3% DMSO concentration. Three technical replicates were performed. The number of alive and dead cells was quantified in each well of the multi-well plate immediately before compound addition and at 24, 48 and 72 hours of treatment by Kinetics of Cytotoxicity and Proliferation assay. Percentages of growth, percentages of dead cells, GI_{50}, TGI, and LC_{50} were calculated at each time point to evaluate reduction of proliferation and induction of cell death, data reported in Table S2.

2.3.7.1. *Cell culture*

A498, A-704, A549, and HT1197 cells were cultured in DMEM high glucose supplemented with 10% FBS, 2 mM L-Glutamine, Non-essential aminoacids, 1 mM Sodium Pyruvate, and Antibiotic Antimycotic Solution. Cells were cultured at 37 °C, 5% CO_2 humidified air.

2.3.7.2. *Kinetics of Cell Proliferation and Cytotoxicity*

24 hours before compound addition, 500 cells suspended in 20 µL phenol-red free complete medium containing SiR-DNA 0.5 µM (Tebu-bio SC007) and CellTox Green Dye 0.8x (Promega G8731) were plated in each well of a 384 Well Flat Clear Bottom Black Polystyrene TC-Treated Microplates (Corning 3764). The day after, 10 µL of serial dilutions of compounds in complete medium were added to each sample to obtain indicated treatment concentrations. Plating of cells, preparation of serial dilutions and addition of compounds to cells were performed using an automated liquid handling platform (Gilson Pipetmax). Immediately before compound addition to cells and after 24, 48 and 72 hours from treatment, images for far-red fluorescence (Cy5 filter), green fluorescence (GFP filter) and phase contrast were taken with objective 4x using automated digital widefield microscopy system BioTek Cytation 5. Cy5 filter: led cube 625nm, filter cube excitation 650 ± 30, emission 800 ± 90. GFP filter: led cube 465nm, filter cube excitation 469 ± 25, emission 525 ± 25. During each reading, cells were maintained at 37 °C, 5% CO_2. For each well, four images were taken and merged to cover the entire well. Number of nuclei stained by SiR-DNA in far-red fluorescence, and number of dead cells stained by CellTox Green Dye in green fluorescence, were automatically counted using BioTek Gen5 software. Alive cells were calculated by subtracting number of dead cells from total count of nuclei.

2.4. Physicochemical, pharmacokinetic and druglikeness predictions

SwissADME (http://www.swissadme.ch) predictions were performed for each final compound. [34] The prediction does not discriminate between *E*- and *Z*-isomer. The physicochemical properties comprise typical molecular characteristics, including the TPSA (Topological Polar Surface Area). Log $P_{o/w}$ is calculated through different methods, and an average value is reported as consensus Log $P_{o/w}$. iLOGP, XLOGP3, WLOGP, MLOGP, SILICOS-IT methods contributed to the averaged Log *P*. [35] The solubility and the Log *S* of each compound are also determined through several methods. Pharmacokinetics properties are represented by the prediction of the GI (gastrointestinal), BBB (blood-brain barrier) and skin absorption, but also the affinity (substrate or inhibitor) for some important proteins (*e.g.* P-gp) and metabolic enzymes. Druglikeness is expressed through different methods, *e.g.* the Lipinski 'rule of five', [36] and the bioavailability score. Other druglikeness predictions were calculated with the Ghose, Veber, Egan and Muegge filters. Final considerations are the synthetic accessibility and the leadlikeness. The latter parameter outline the similarity of structure and physico-chemical properties with a definable "lead" compound.

3. Results and Discussion

3.1. Molecular Docking

In order to evaluate the feasibility and the benefit of the fluorine substitution on the benzotriazole moiety, molecular docking simulations were performed ahead of the synthetic efforts. Aiming to compare their binding affinity with the tubulin active site, colchicine as a known ligand, compound **34** and the corresponding newly designed difluoro-derived compound (labelled derivative **9b**) were docked in the colchicine-binding site on tubulin. The X-ray structure of tubulin co-crystallised with colchicine, PDB ID: 4O2B, was selected. Colchicine was removed from its binding pocket in tubulin and re-docked in the same binding pocket with the same coordinates, showing affinity energy of -9.8 kcal/mol. The same protein structure, without colchicine in place, was employed for docking studies on compounds **34** and **9b**. The best-docked pose for derivative **34** presented a binding energy value of -6.7 kcal/mol, meanwhile the best-docked pose of compound **9b** ranked affinity energy of -8.6 kcal/mol. All dockings were analysed with PyMOL, [37] Maestro [38] and LigPlot. [39] As depicted in Figure 2, **9b** has two F···N electrostatic interactions, better-called fluorine bonds, [40] involving the electron-acceptor fluorine in position 5 on the benzotriazole scaffold (depicted in Figure 2B as green dashes). These dipole-dipole interactions involve intrinsic nitrogen atoms of Cysβ241 and Leuβ242 (~4 Å). Leuβ242 contributes also with hydrophobic interactions between the carbons of the isobutyl side chain of the amino acid (aa) and the benzotriazole carbons. The benzene moiety of the benzotriazole provides hydrophobic interactions with Alaβ250, Aspβ251 and Leuβ255, while the side-chain benzene moiety establishes van der Waals interactions with aas located in the opposite portion of the binding pocket: Leuβ248, Gluα183, Lysβ254 and Asnβ258. The amidic nitrogen atom of Asnα101 interacts with the acceptor oxygen of the methoxyl group of compound **34**, forming a hydrogen bond (4.18 Å, Figure 2A). The best binding pose of derivative **9b** showed the methoxyl group in a different conformation if compared with **34**; accordingly, this determinates only a weak interaction with the same asparagine residue. Moreover, the carbon atom of the methoxyl group contributes to the binding with a hydrophobic interaction with Lysβ254.

Then, colchicine was re-docked in its binding pocket. The eptacyclic (tropolone) ring has a hydrophobic interaction with Alaα180. Trimethoxyphenyl moiety of colchicine is oriented towards the hydrophobic portion of the tubulin-binding pocket. Metβ259, Asnβ258, Leuβ255, Lysβ254, Aspβ251, Alaβ250, Leuβ248, Leuβ242 and Cysβ241 are the representative aas of this portion of the pocket. Most of these aas also establish hydrophobic interactions with compound **9b**, especially with the heterocyclic scaffold of the molecule, but also with the acrylonitrile linkage, as shown in Figure 2B. Figure 3 shows polar and hydrophobic interactions among compound **9b** and α- and β-tubulin subunits in the colchicine-binding pocket. Methoxyl group is shown to be the most solvent-exposed portion of the molecule, pointing toward the outer portion of tubulin active site.

In the binding pocket, four aas (Serα178, Thrα179, Alaα180, Alaα181) were recognised to be crucial for the binding of colchicine. Using AutoDockTools, [30] these aas residues were set as flexible during the docking calculations. Compound **34** best-predicted pose showed an affinity energy value of -6.7 kcal/mol, meanwhile, compound **9b** presented a ranked affinity energy of -7.4 kcal/mol. This preliminary docking prediction suggests that compound **9b** possesses a good binding profile and that the difluoro substitution on the main benzotriazole scaffold, could be considered beneficial for the affinity to the colchicine-binding site of tubulin, pushing us forward to continue our work. Therefore, the new series of (*E*)(*Z*)-2-(5,6-difluoro-(1*H*)2*H*-benzo[*d*][1,2,3]triazol-1(2)-yl)-3-(*R*)acrylonitrile

derivatives was designed, synthesised and tested *in vitro* on different tumour cancer cells, as further reported in the present work.

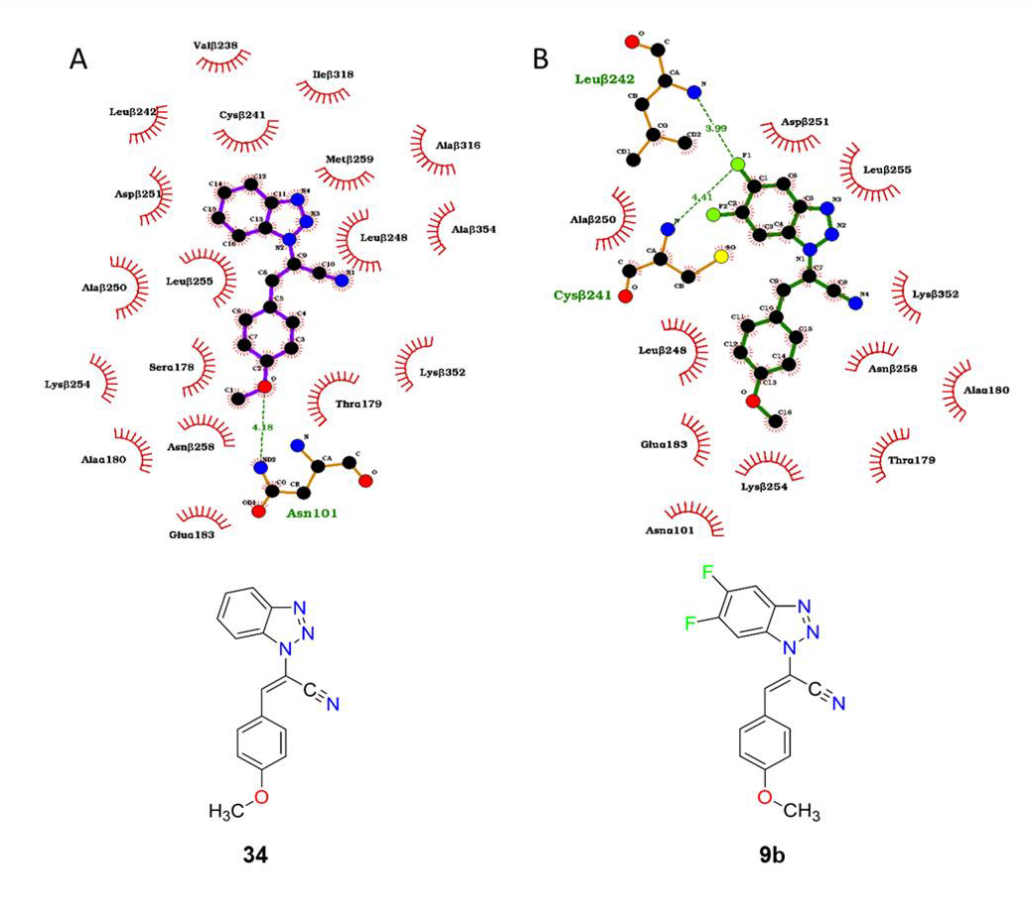

*Figure 2. Schematic comparison between the binding pose of compounds **34** (A) and **9b** (B) inside the tubulin-binding pocket. H-bonds are depicted as green dashed lines and hydrophobic contacts as red hash marks. Atom colours: carbon, black; nitrogen, blue; fluorine, green; oxygen, red. Amino acids are labelled with the residue name, the chain and the correspondent number. The hashes in the ligand show atoms having hydrophobic interactions with aas. Distances are given in Å. Figure made by using LigPlot*$^{+}$. [39]

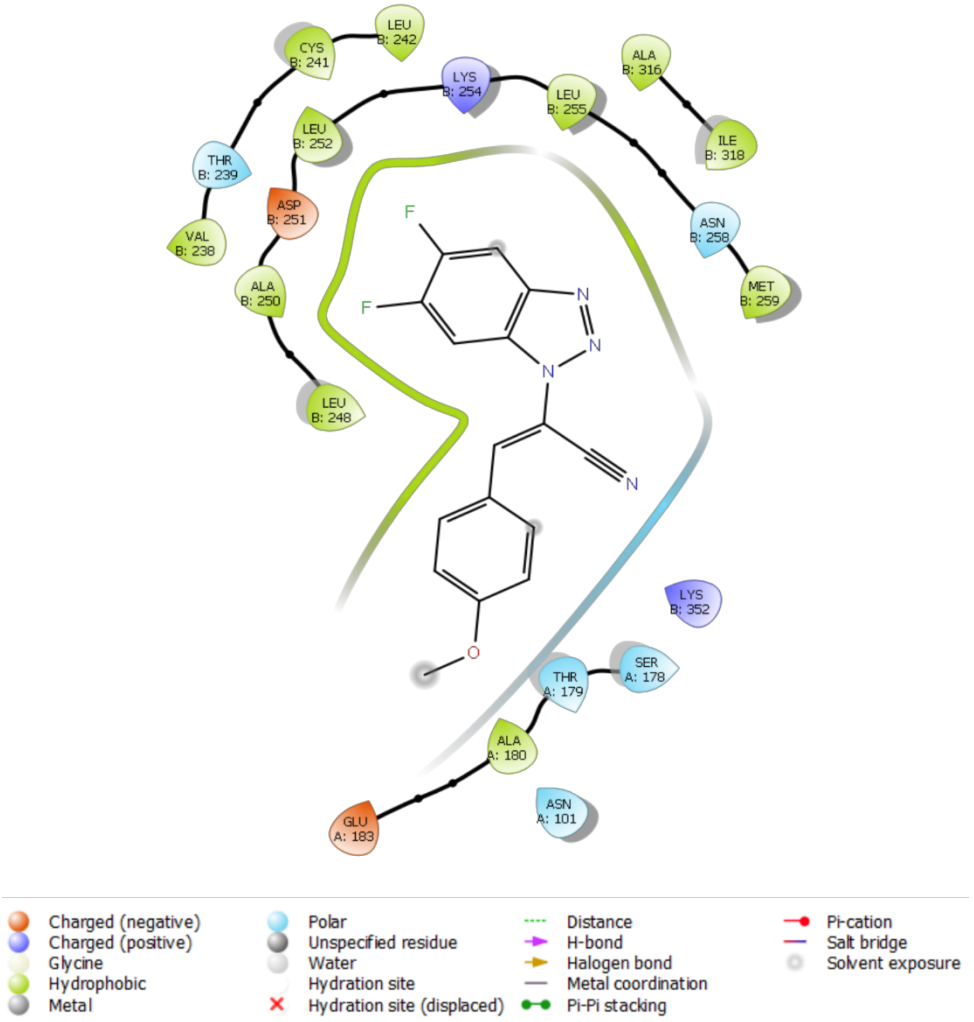

Figure 3. Ligand Interaction Diagram and LID legend of the different interactions between compound ***9b*** *and different amino acids in tubulin binding pocket. Residue markers are coloured according to residue type (green = hydrophobic, cyan = polar, red = negative, purple = positive). Green and cyan lines represent the interactions between* ***9b*** *and the different portions of the binding pocket. The gap in the line shows the opening of the pocket. Grey atom markers on the background of ligand structure represent the solvent-accessible surface area (SASA) of that atom, and the marker size represents the amount of exposure. Each protein residue is depicted as a "guitar pick": it points away from the ligand when the aa backbone faces towards the ligand, or it points to the ligand when the aa side chain faces towards the ligand. Cut-off default of 4 Å was used. Figure made by using Maestro.* [38]

3.2. Chemistry

The synthetic route followed to synthesise final compounds **9a-j**, **10e**, **11a**,**b and 13d-j** is described in Scheme 1A, B. The synthesis, as depicted in Scheme 1A, started with the commercially available 3,4-difluoroaniline (**1**), which was in first place acetylated, affording compound **2**. The following nitration, hydrolysis and reduction led to 4,5-difluorobenzene-1,2-diamine (**5**), which was cyclized with $NaNO_2$ in HCl, obtaining the 5',6'-difluorobenzotriazole **6**. Reaction of **6** with chloroacetonitrile ($ClCH_2CN$), carried out in the presence of KOH, yielded the geometric isomers **7a**,**b** bearing an acetonitrile chain on the triazole ring (Scheme 1A).

As a final step (Scheme 1A), the Knoevenagel condensation between each acetonitrile isomer (**7a**,**b**) and the appropriate commercial aldehydes (**8a-j**), afforded the final (*E*)(*Z*)-2-(5,6-difluoro-(1*H*)2*H*-benzo[*d*][1,2,3]triazol-1(2)-yl)-3-(*R*)acrylonitrile derivatives **9a-j**, **10e**, and **11a**,**b**. Knoevenagel condensation generally provided the sole *E*-isomer. In some cases, the reaction generated also the *Z*-isomer in very low quantity, In some cases, the reaction generated also the *Z*-isomer in very low quantity, not sufficient to be fully characterised (as explained in Paragraph 1.1 for compound **9i**). *Z*-isomer isolation from the reaction mixture was possible only for the compound (**10e**). The reaction was performed by one out of three different synthetic conditions: (1) TEA (triethylamine) in toluene (as previously described by us [18–23]); (2) DIMCARB (dimethylammonium dimethylcarbammate) used as base and reaction catalyst, in acetonitrile and (3) piperidine in acetonitrile (Scheme 1A). The presence of DIMCARB (in CH_3CN) also allowed to obtain the *p*-NO_2-derived *Z*-isomer **10e**, while using TEA (in toluene) as base provided the *E*-isomer **9e** as the major product. Compounds **13d,j** were obtained by Knoevenagel condensation between the 2-(1*H*-benzo[*d*][1,2,3]triazol-1-yl)acetonitrile isomer, synthesised as previously reported, [23] and the appropriate aldehydes **8d**,**j** (Scheme 1B). The substituents on the acrylonitrile moiety were selected based on the antimitotic activity properties of the series of compounds previously reported by us [18–23] or by colleagues. [41] As two new substituents were selected from the literature (4-hydroxyphenyl and isoquinolin-5-yl), we also designed and synthesised new parental compounds of the lead **34**, thus two new (*E*)-2-(1*H*-benzo[*d*][1,2,3]triazol-1-yl)-3-(*R*)acrylonitrile derivatives (**13d**,**j**), as new parental compounds of the lead **34**.

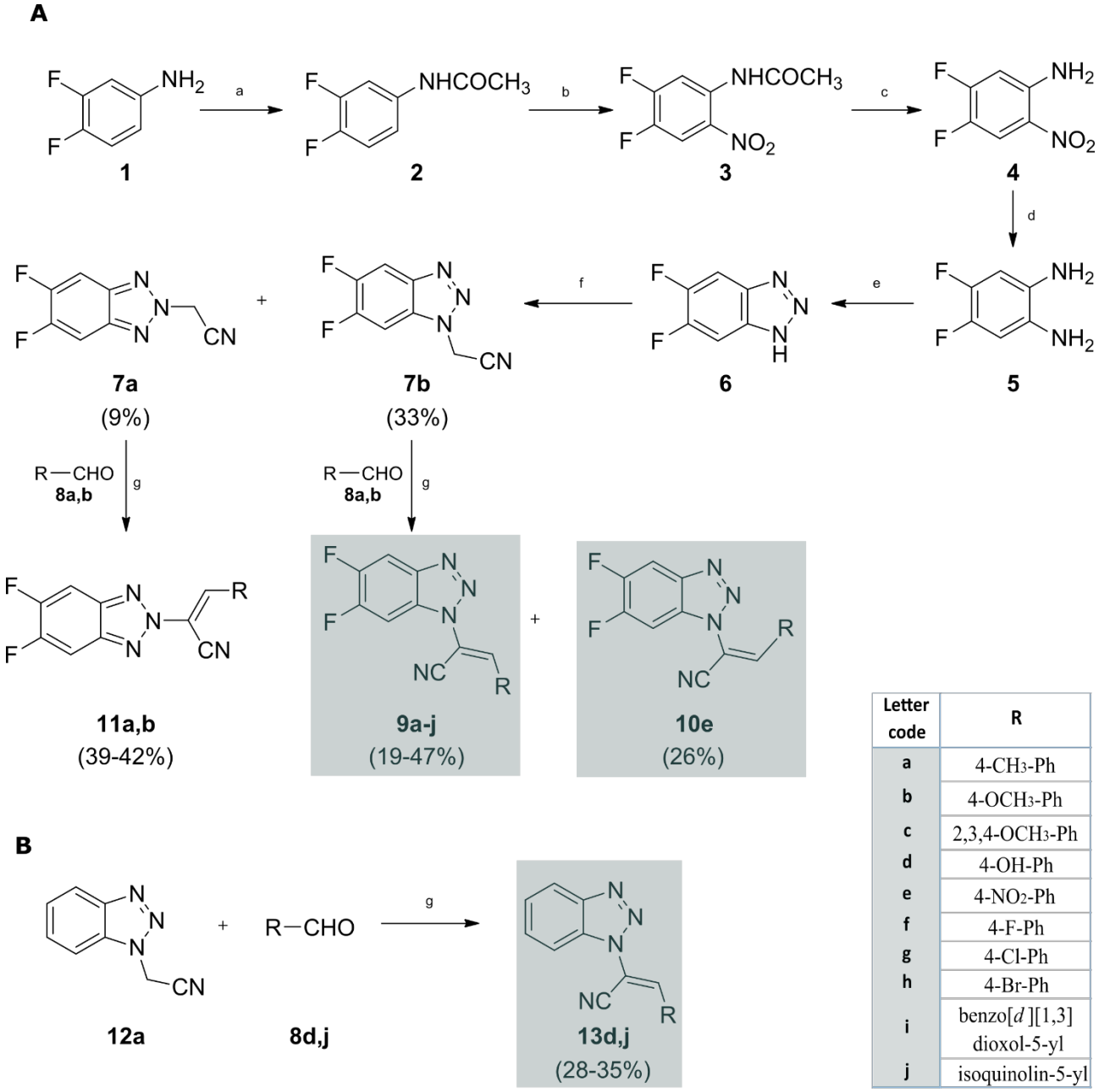

*Scheme 1. (**A**) Synthesis of (E)(Z)-2-(5,6-difluoro-(1H)2H-benzo[d][1,2,3]triazol-1(2)-yl)-3-(R)acrylonitrile (**9a-j**, **10e**, **11a,b**) and (**B**) (E)-2-(1H-benzo[d][1,2,3]triazol-1-yl)-3-(R)acrylonitrile derivatives (**13d,j**).* Reaction conditions: (a) $(CH_3COO)_2O$, 10 min, 0 °C; (b) KNO_3, H_2SO_4, 2h, r.t.; (c) H_2SO_4 conc, 2h, reflux; (d) H_2, Pd/C, 2 h, r.t.; (e) $NaNO_2$, HCl, 20 h, r.t.; (f) $ClCH_2CN$, KOH, DMF, o/n, reflux; (g): (1) TEA, toluene, 110 °C, or (2) DIMCARB, CH_3CN, 60 °C or (3) piperidine, CH_3CN, 60 °C; properly chosen to get the full conversion.

3.3. Biology

3.3.1. NCI60 in vitro screening

In order to evaluate the potential anticancer profile of our compounds, we firstly focused on their antiproliferative ability in cancer cells. The first *in vitro* anti-cancer screening was performed through

the NCI60 test (NCI, Bethesda, USA). In the beginning, a single high dose of 10 μM of the compound was tested on the full NCI60 cell panel. The panel comprises a set of different cancer lines including solid (non-small cell lung, colon, central nervous system - CNS, ovarian, renal, prostate, breast cancers, and melanoma) and haematological (leukaemia) tumours. Results showed that, at 10 μM concentration, 5',6'-difluoro-substituted 1*H*-benzotriazole derivatives (**9a-j**, **10e**) possess higher percentages of growth inhibition (GI) in comparison to 2*H*-benzotriazole derivatives (**11a,b**). All data from NCI60 are reported in Supplementary Material (Figures S34-53). Among all the new synthesised derivatives, compounds **9a**, **9e**, **9g** and **9h** satisfied the pre-determined threshold inhibition criteria in a minimum number of cell lines and progressed to the second step of the 5-dose assay, from 100 μM to 10 nM. Among them, derivative **9a** exhibits GI values in the range 60-100% against all the sixty solid and haematological cell lines, reaching GI percentages around 100% against all leukaemia cell lines. More in depth, compound **9a** turned out cytotoxic against seventeen solid and haematological tumour cell lines with lethal percentages up to 90% (U251, CNS cancer cell line). At 1 μM, compound **9a** presents GI percentages ranging from 40 to 60% against eight tumour cell lines and 70-100% against further seven cell lines (93% against NCI-H522 cell line of non-small cell lung cancer). General GI_{50} values are up to 0.1 μM, while LC_{50} and TGI values come up to 1 μM.
In conclusion, compound **9a** showed the best scores and was selected as lead of this series. Antiproliferative activities of **9a** on NCI60 cancer cells are reported in Figure 4.

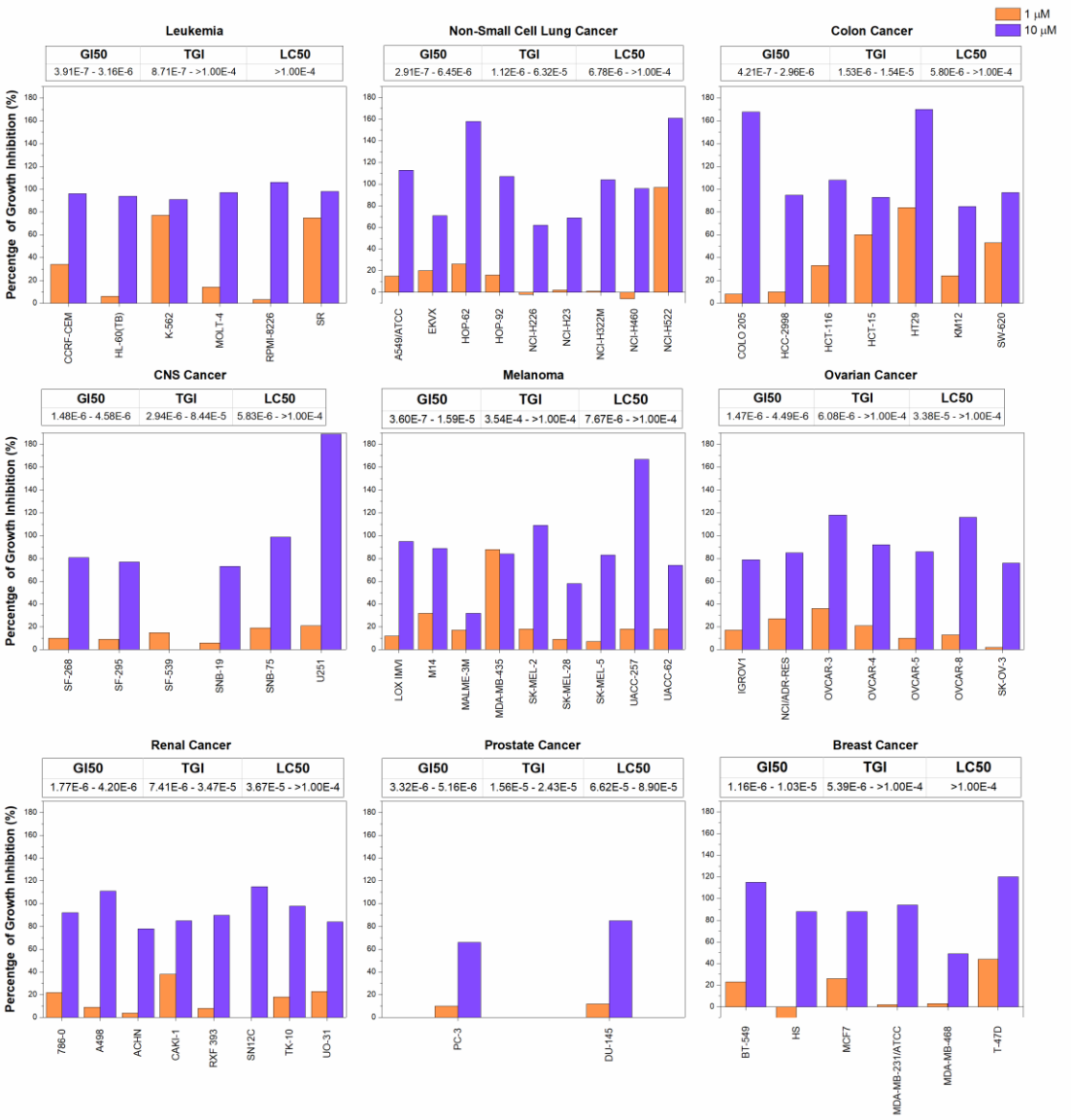

Figure 4. Graphical illustration of antiproliferative activity for compound ***9a*** *tested against NCI60 cell panel. Percentage of Growth Inhibition (%) is reported for each cell line tested, grouped for type of cancer. For each group, a range of* GI_{50}*, TGI and* LC_{50} *are reported; values are expressed as molar concentration (M).*

Regarding 1*H*-benzotriazole derivatives (**13d,j**), compound **13d** demonstrated a low GI rate, but, contrariwise, isoquinolin-5-yl derivative **13j** showed an interesting antiproliferative activity and was selected for the 5-doses dilution assay. At 10 µM, **13j** was able to inhibit the proliferation of the majority of tumour cell lines with percentage values ranging between 70 and 100% (some of them are reported in Figure 5). At 1 µM, Compound **13j** showed antiproliferative activity against six cell lines belonging to four different tumours type (Figure 5), exhibiting growth inhibition percentages of 50-60% against most of the reported cell lines. However, **13j** showed the best activity against CCRF-CEM leukaemia line, inhibiting completely the tumour cell growth.

In light of the reported results for all the newly synthesised compounds (Figures 4,5 and Figures S34-53), **9a** showed an overall better antiproliferative potency and a wide range of activity. Hence, derivative **9a** was selected as lead compound for further biological assessments.

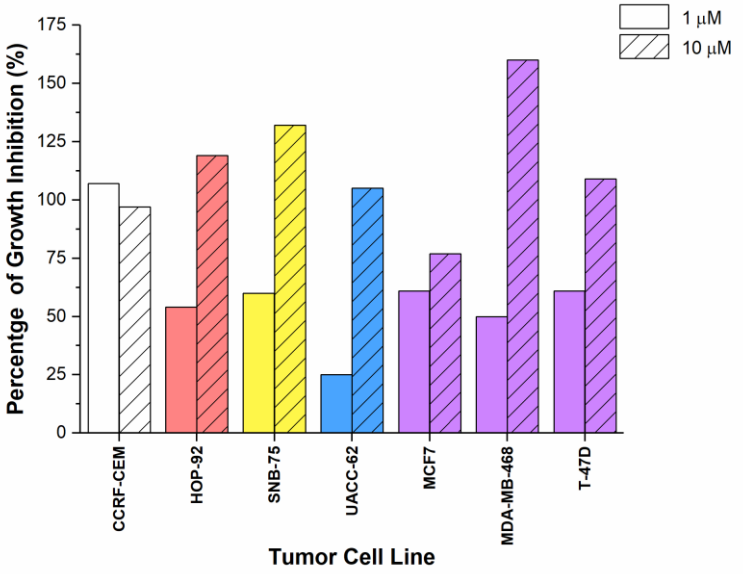

	GI50	TGI	LC50
Leukemia	2.53E-7 - 3.21E-6	2.43E-5 - >1.00E-4	>1.00E-4
NSC Lung Cancer	5.32E-7 - 2.32E-5	5.13E-6 - >1.00E-4	>1.00E-4
CNS Cancer	1.84E-7 - 3.24E-5	3.61E-6 - >1.00E-4	>1.00E-4
Melanoma	2.04E-6 - 7.71E-6	>1.00E-4	>1.00E-4
Breast Cancer	5.57E-7 - 2.97E-6	2.84E-6 - >1.00E-4	>1.00E-4

*Figure 5. Graphical illustration of representative antiproliferative activity results for compound **13j** tested against NCI60 cell panel. Seven cell lines were selected and reported coloured by type of cancer. The bar chart reports the percentage of Growth Inhibition for each cancer cell line when treated with **13j** at 1 or 10 μM concentration. The table shows a range of GI_{50}, TGI and LC_{50} values (M) for each reported type of cancer.*

*3.3.2. IC_{50} and Mechanism of action of compound **9a** against HeLa cells*

In order to understand if **9a** could be defined as a microtubule destabilising agent (MDA), as well as its previously reported for analogue compounds, [21,22] its antiproliferative activity was tested against HeLa cells through XTT assay. XTT is a colorimetric assay useful to analyze the number of viable cells by the ability their metabolic activity: tetrazolium salts added to the culture medium are actively absorbed into cells and reduced by dehydrogenase enzymes of metabolically active cells to yield a chromogenic formazan product. Cells were treated at different concentrations of **9a** ranging between 0.1 and 5 μM, DMSO was used as control. XTT assay was carried out after 24 and 48 hours of treatment, the absorbance data were obtained and processed to calculate the percentage of cell viability. [42] A reduction of 50% of alive cells was detected after 48 hours of treatment with **9a** with an IC_{50} value of 3.2 μM.

To prove that **9a** was able to affect the HeLa cell cycle, flow cytometry was used to evaluate the changes in the DNA content after treatment. As shown in Figure 6, the administration of **9a** at 5 μM causes an increase of cells number in G2/M-phase (54%) compared to the control (30%) after 24 hours of treatment. This effect was even more evident at a higher concentration of 10 μM with a percentage of G2/M-phase cells of 66% after 24 hours. The increase of cells in G2/M-phase causes a

contemporary decrease of G1-phase cells both at 5 µM (39%) and 10 µM (20%) compared to the control (65%). Results after 48 hours showed slight recovery of cells in G1-phase at 5 µM (41%), but a dramatic increase of cells in G2/M-phase (87%) proportional to the decrease of G1-phase rate (10%) after 48 hours of treatment at 10 µM.

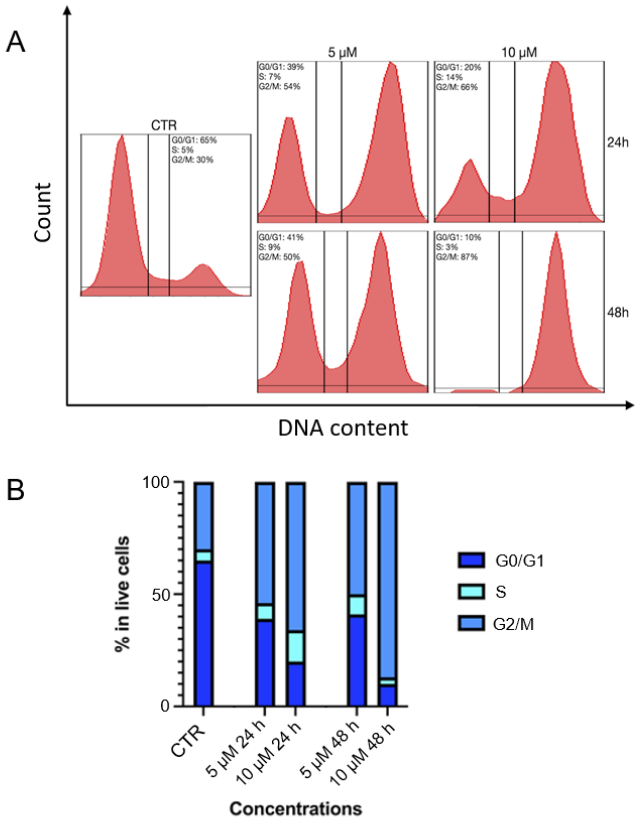

*Figure 6. Cell cycle phase distribution in HeLa cells after **9a** treatment. **A.** Representative cell cycle profiles of HeLa cells treated with 5 µM or 10 µM of **9a** for 24 or 48 h. Treatment with 5 µM of **9a** causes an accumulation of cells in G2/M phase after 24 hours with a completed block at 10 µM after 48 hours post-treatment. **B.** Percentages of cells in the different phases are shown.*

*3.3.3. Compound **9a** slows the cytokinesis in HeLa cells*

Aiming to confirm the cell cycle impairment observed in Figure 6, we performed a fluorescence microscopy screening on HeLa cells treated with **9a** for 48 hours. Based on the previously described cell accumulation in G2/M phase we decided to count the number of incomplete cytokinesis events per field. As shown in Figure 7A,B, the amount of incomplete cell divisions increases starting from 0.3 µM compared to controls. We also observed an overall increase in cell dimension compared to controls (mock, untreated).

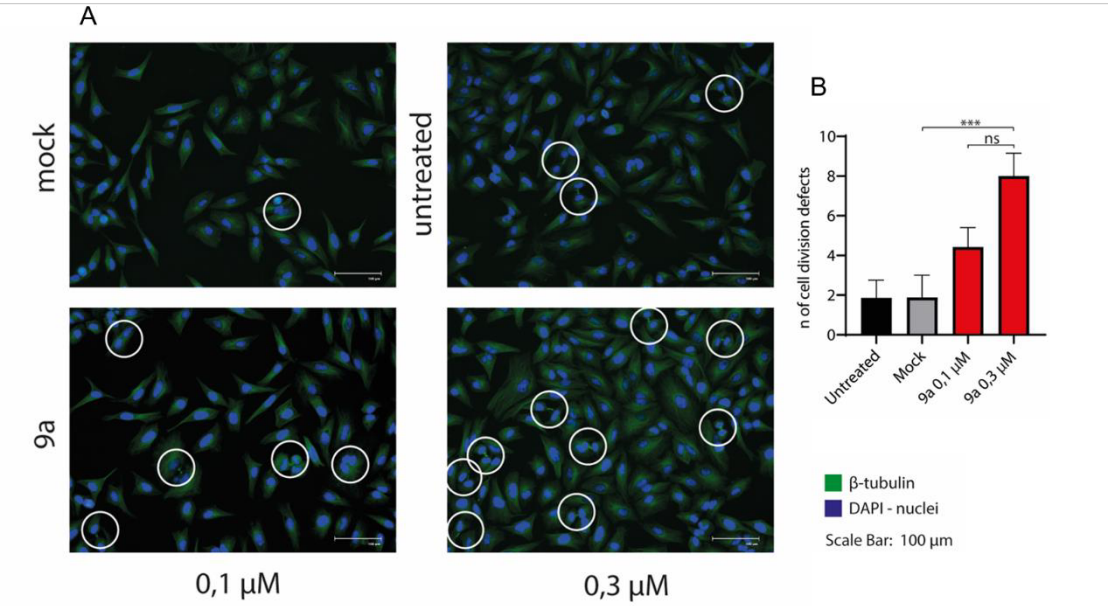

Figure 7. Fluorescence microscopy screening of cytokinesis. ***A.*** *Images, taken 48 h treatment with* ***9a*** *and controls stained with β-tubulin, show an increase of incomplete cell divisions starting from 0.3 µM.* ***B.*** *Kruskal-Wallis test with multiple comparisons performed on the number of incomplete cell division per field.* *** *P(*<0,0001); ns = not significant.

3.3.4. High-Content Imaging on HeLa cells

In order to gain insights in the potential targeting of microtubules elicited by **9a**, we analysed tubulin behaviour in a cellular setting in the presence of our lead compound. Briefly, HeLa cells were treated for 24 hours with **9a** at various concentrations (10, 25, 50, 100 and 500 nM). Cells were then stained for β-tubulin and processed using high-content confocal microscopy screening. As shown in Figure 8, we observed β-tubulin disassembly starting from 50 nM. At the same concentration, the high-content screening revealed that HeLa cells increased dimension by three times compared to controls (Figure 8B). This phenomenon indirectly confirms the cell-cycle blockade observed in Figure 6. The increased cytoplasmic area is compatible with senescent-like phenotype.

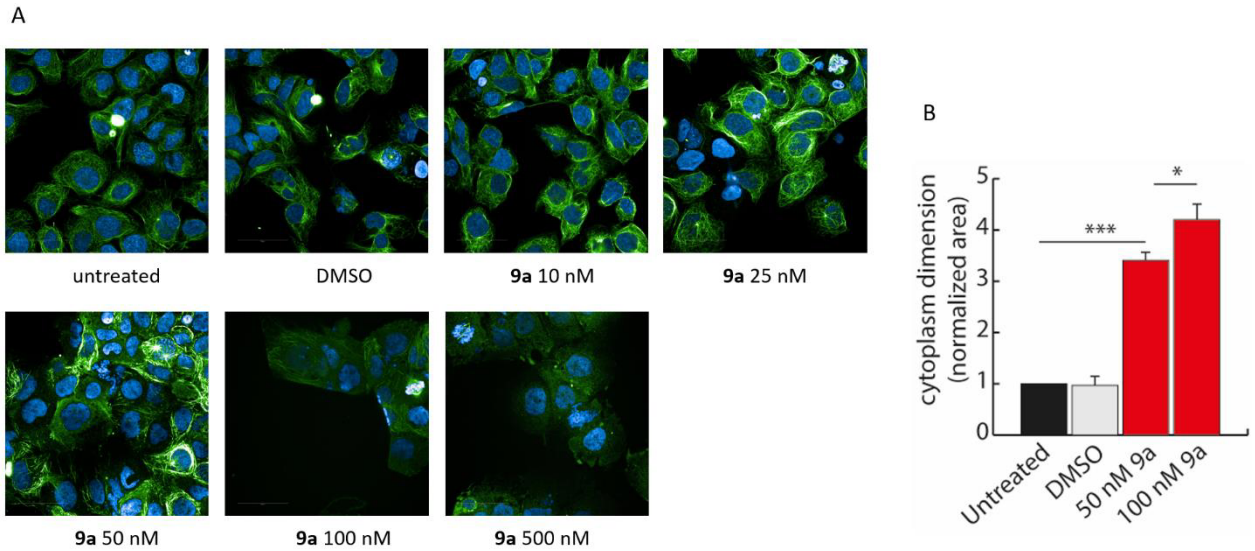

Figure 8. High content confocal screening of HeLa cells. **A.** Increasing doses of **9a** were used to treat HeLa cells for 24 h. Then, cells were stained for β-tubulin (green) and nuclei (DAPI-blue). Starting from 50 nM we observed the disruption of microtubules. **B.** One way ANOVA analysis performed on cytoplasm area using high-content screening. Data are expressed as mean ± SD. Experiments were performed with three biological and three technical replicates.

*3.3.5. Cytotoxicity evaluation of compound **9a** in presence or absence of extrusion pump inhibitor (EPI)*

Extrusion pumps (EPs) represent one of the main issues in anticancer therapy since they are often overexpressed in drug-resistant cancer cells. In order to investigate whether this chemical class of molecules could be client of EPs, we tested our lead compound **9a** in cell-based association assay. Four cancer cell lines with EPs overexpression were selected. [43] Two kidney cancer (A498, A-704), one non-small cell lung cancer (A549) and one bladder cancer (HT1197) cell lines were selected for this experiment. Two of them, A498 and A549 cell lines were already used in the NCI screening and the results from the NCI60 cell line screening were used to select a concentration range of compound **9a** to be used in the association assay. The four cancer cell lines were treated with the sole derivative **9a** or in association with an extrusion pump inhibitor (EPI) from our group library, compound here labelled as **SS26**. Compound **SS26** (structure not showed for Intellectual Property rights) EP inhibition activity was previously validated by association with Doxorubicin (a know EP client) in HCT-15 colon cancer cell line, as shown in Figure S54. The association assay results are reported in Figure 9 and Figure S55 and S56. Figure 9 shows the Percentage of Growth (%) for each tumour cell line, at each time point at 5 different concentration of compound **9a** (1, 2, 4, 8 and 16 μM), alone and in association with our EPI at a fixed concentration (1 μM). The data are reported as Loess model with 95% confidence interval. The data collected at 24 hours time-point are presented for completeness but were not considered for the cytotoxic effect analysis since the cell growth is not yet stable at 24 hours after seeding. The results of the experiment at 48 and 72 hours clearly highlight that the association with EPI **SS26** resulted beneficial for the antiproliferative activity of **9a** against all the 4 tested tumour cell lines. The most striking results were obtained after 72 hours of treatment for all the tested cell lines. The cell growth inhibition was highly increased when **9a**+**SS26** were tested against A-704 cell line at both 48 and 72 hours. The most representative data concerned the two concentrations of 4 and 8 μM of compound **9a** since at 16 μM concentration the cells were saturated and the EPI effect was not detectable any longer. Figure S55 presents the raw cell growth values, while Figure S56 shows in bar charts the concentration-dependent efficacy.
We obtained two main pieces of information from this association assay: i) we proved that these small molecules are client of extrusion pumps with a negative effect on the antiproliferative activity; ii) we demonstrated that, by increasing the concentration of derivative **9a** in the cytosol, the antiproliferative activity is potentiated.

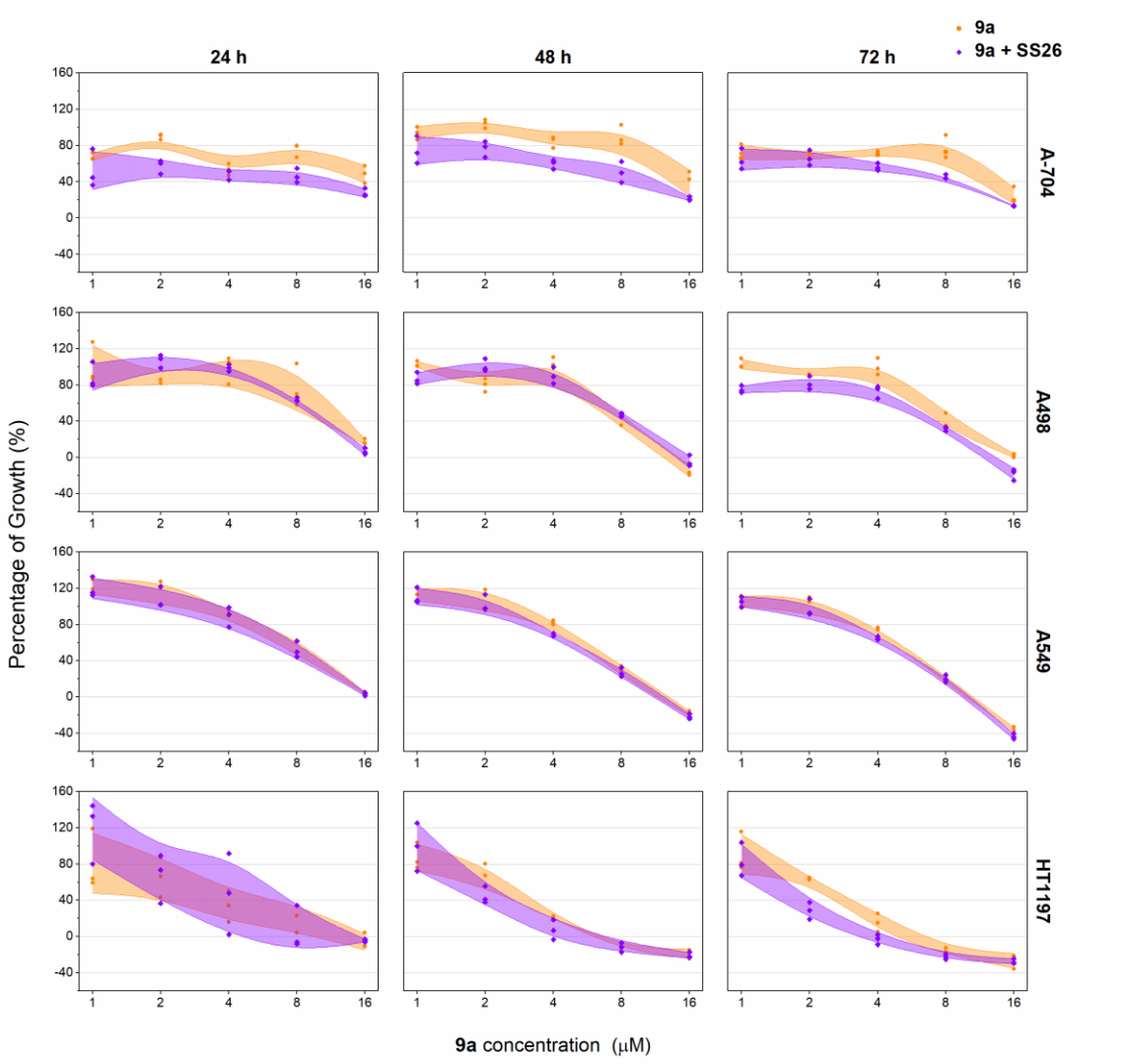

*Figure 9. Association assay. Percentage of Growth in cells treated with compound **9a** alone and in association with EPI **SS26**. Loess model, 95% Confidence interval.*

*3.3.6. Compound **9a** docks in the colchicine-binding site on tubulin*

As a result of the biological assessments previously reported, derivative **9a** was selected as the lead compound of this series of molecules. Molecular docking studies were conducted on **9a** in the colchicine-binding site on tubulin, using the same docking parameters and procedures already followed for colchicine, compounds **34** and **9b**. Docking calculations evidenced the role of the fluorine bonds: the fluorine atom in position 6 established two different bonds with the amino groups of Alaβ250 (4.75 Å) and Leuβ255 (4.96 Å) of β-tubulin. Moreover, the oxygen of Valβ238 of β-tubulin engages in H-bond with the N_3 in the benzotriazole nucleus of **9a** (4.28 Å), while the carbonyl oxygen of Ala317 of β-tubulin interacts with the cyan group of the acrylonitrile linker of **9a** (4.29 Å). Compound **9a** also establishes different nonpolar interactions in the colchicine binding site, especially with the β-subunit of tubulin. In particular, the benzotriazole scaffold mainly interacts with the aa residues Aspβ251, Ileβ318 and Alaβ354, while the tolyl moiety establishes hydrophobic interactions with Leuβ248, Asnβ258, Metβ259 and Lysβ352. Figure 10 illustrates the docking conformation of compound **9a**.

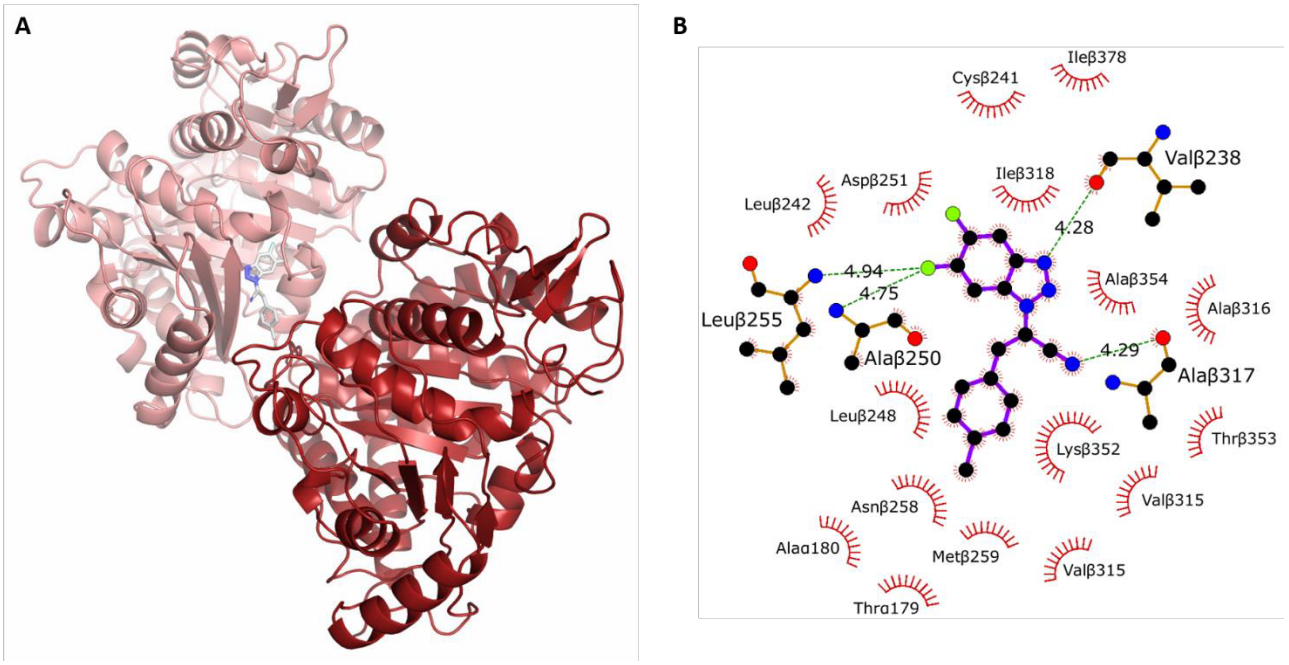

Figure 10. 3D structure of the docking pose of ***9a*** *in the colchicine-binding site in tubulin.* 2D representation of lead compound **9a** showing its polar/nonpolar interactions with the colchicine-binding pocket on tubulin.

Then, the conformation state of the top-ranked pose of compound **9a** was superimposed with the crystal structure of colchicine in its binding site, at the interface of α- and β-tubulin. As shown in Figure 11, the benzotriazole scaffold occupies the trimethoxyphenyl portion of the colchicine-binding site, while the CH_2-CN chain almost overlaps with one of the methoxy groups located in the same aromatic portion. Additionally, the tolyl moiety of **9a** overlaps with the phenoxy ring of colchicine (Figure 11). Overall, our results suggest that the favourable binding mode of lead compound **9a** docks similarly to the crystal structure of colchicine in its binding pocket of the α,β-tubulin dimer.

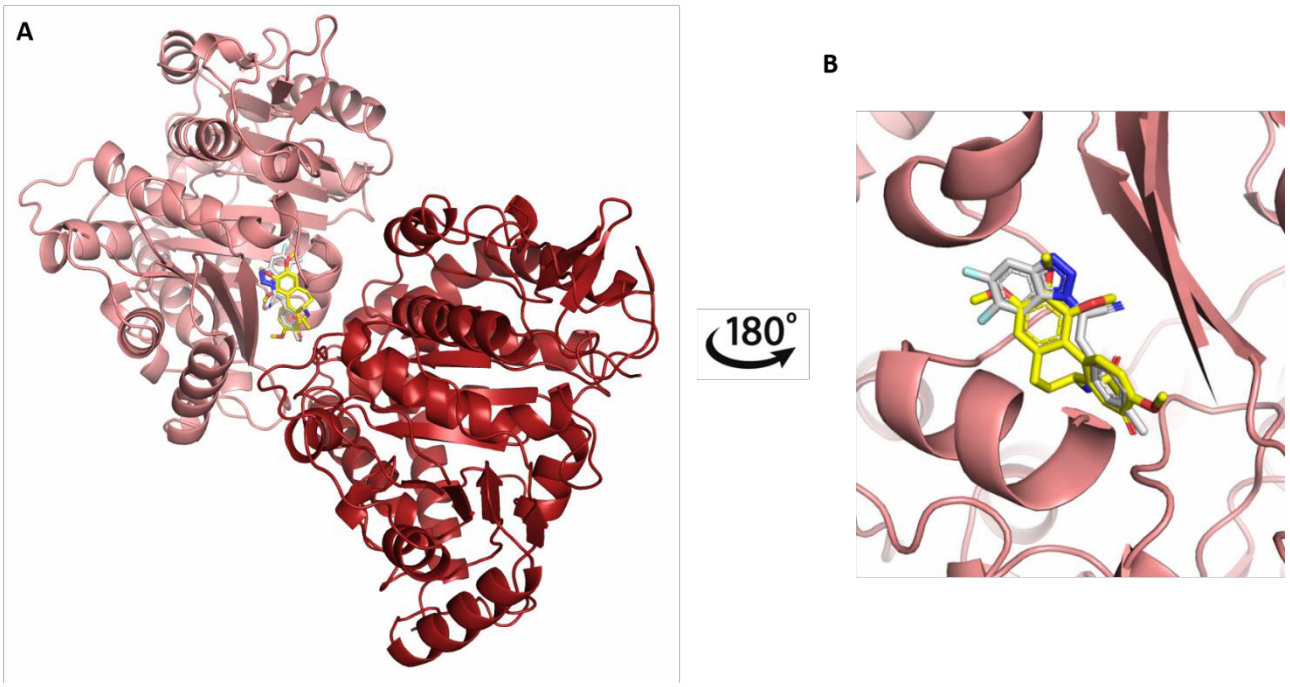

*Figure 11. Superimposition of the binding pose of compound **9a** (light grey) and the crystal structure of colchicine (yellow, PDB ID: 4O2B) in the colchicine-binding pocket at the interface of α- and β-tubulin.* Tubulin α,β-chains are distinguished by different colours: the β-monomer is salmon-coloured, the α -one is in brick red tonality.

To gain further insights, we decided to compare the mode of binding of the new proposed CBSI **9a** with some of the most important and well-known CBSIs actually in clinical trials (phase I, II or III). In Figure 12, we underlined the difference in binding mode and affinity to tubulin of the different studied molecular structures: compound **9a**, tivantinib (TIV, PDB code: 5CB4), [44] plinabulin (PLI, PDB code: 5C8Y) [44] and crolibulin (CRO, PDB code: 6JCJ). [45] Tivantinib (TIV) is a well-known CBSI in phase I/II/III clinical trials for the treatment of different tumor form. [46–48] The direct binding of TIV to the colchicine-binding site was recently described [49] and the analysis of the tubulin–TIV crystal structure evidenced how TIV binding site and mode overlap with that of colchicine. In particular, TIV establishes several direct H-bonds with Asnβ256 Alaβ315 of β–tubulin, but also interacts with Leuβ246 and Thrα179 via water molecules. [44] Plinabulin is a vascular disrupting agent with depolymerising activity, currently in phase I/II for the treatment of several types of cancer. [50,51] The tubulin–plinabulin co-crystallised structure shows that the small molecule binds a deeper portion of β-tubulin, where it engages in H-bonds with Gluβ198 and Valβ236, and interacts with Glyβ235 and with Thrα179 via water molecules. Also the crystal structure of plinabulin could be overlapped with the one of colchicine. [44] Finally, crolibulin is a chromene-derived inhibitor of tubulin polymerisation, able to affect the cell cycle in G2/M phase. [52] Although it has completed phase I and phase II trial for anaplastic thyroid in co-administration with cisplatin, [53,54] its therapeutic application includes prostate adenocarcinoma [55] and gliomas. [56] Unfortunately, its clinical use is limited due to cardiovascular and neurotoxicity. [57,58] In the tubulin-crolibulin crystal complex, crolibulin occupies the well-known colchicine-binding site, forming three H-bonds

between the 2-amino, 7-amino and 3-cyano groups of the chromene moiety of crolibulin and the aminoacids Thrα179, Alaβ248, respectively.

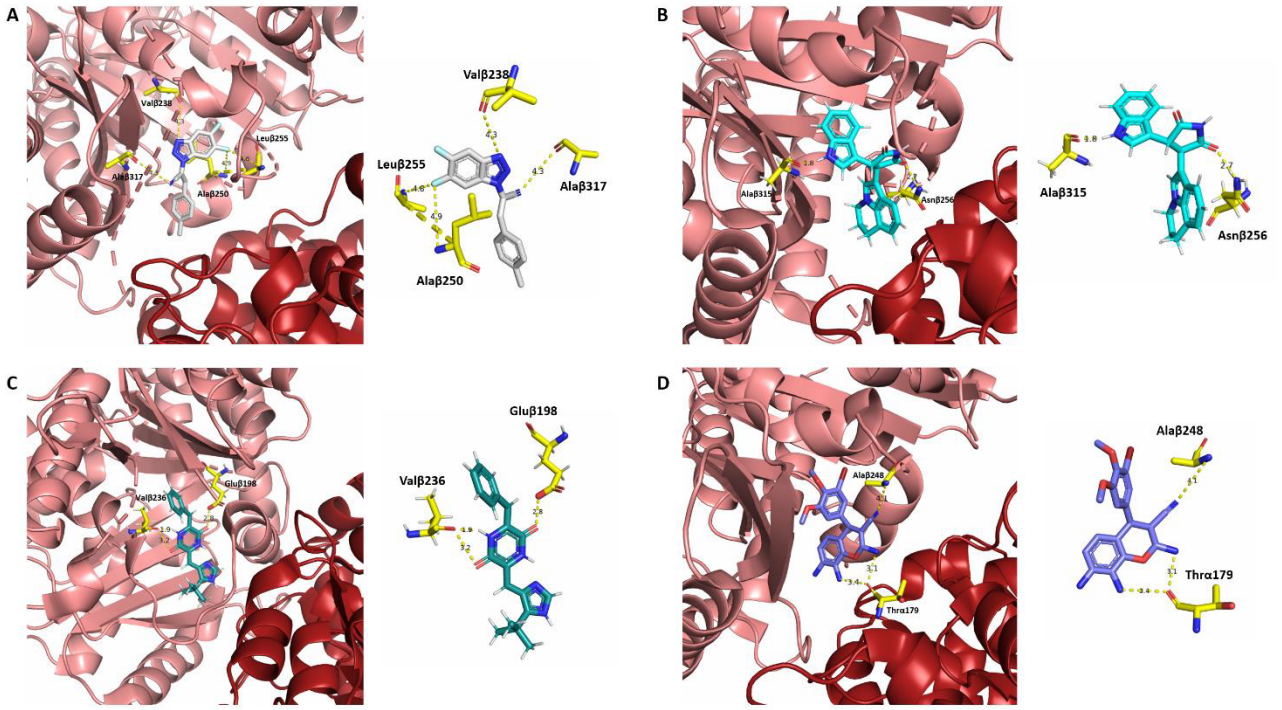

Figure 12. Comparison of binding conformation of the best docking pose of compound ***9a*** *(light grey, A, with 4O2B apo-form) and the crystal structures of tivantinib (blue marine, B, 5CB4), plinabulin (dark green, C, 5C8Y) and crolibulin (violet, D, 6JCJ).* The α-tubulin portion is coloured in brick red, while β-tubulin is salmon-coloured.

As aforementioned, the lead **9a** docks mainly in the β-subunit at the interface between α,β-dimer and engages four main electrostatic interactions with two alanine, one leucine and one valine residues. Although some of the crystal structures of the selected CBSIs overlap with colchicine (Figure 12), the most favourable conformational state of **9a** binds the colchicine-binding pocket in a slightly different way (Figure 11), giving a new pattern of electrostatic/hydrophobic interactions, and indicating **9a** as an interesting compound to be further investigated.

4. Conclusions

In summary, in this work we developed a series of 5',6'-difluorobenzotriazolacrylonitrile derivatives and we reported computational and experimental data suggesting them to act as MDAs. More in depth, we demonstrated, through molecular docking studies, the different polar (fluorine bonds with cysteine and leucine residues, H-bonds, *e.g.* with different leucine residues) and nonpolar (with the hydrophobic portion of the pocket) interactions between the representative compound **9b** and the tubulin binding site. The binding mode of **9b** was also compared to the best-docked poses of colchicine and compound **34**. *E*/*Z*-designed derivatives (**9a-j**, **10e**, and **11a**,**b**, **13d**,**j**) were obtained through Knoevenagel condensation as a final step of the synthetic route and properly characterised

through NMR spectroscopy analysis. Then, all compounds were subjected to a preliminary *in vitro* screening against the NCI60 cancer cell lines to evaluate their potential anticancer profile. As we noticed from our previously developed compounds, [18–22] the results confirmed that 1*H*-benzotriazole derivatives (**9a-j**, **10e**) possess a better profile activity than 2*H*-benzotriazole ones (**11a**,**b**). Overall, *in vitro* results suggested the *p*-CH_3 derived compound **9a** as the most active compound: at 1 μM concentration, it showed GI percentages between 40 and 60% against eight tumour cell lines and 70-100% against further seven cell lines. On this basis, derivative **9a** was selected as lead compound of this library of molecules to be subjected to further investigations. To prove its activity as MDA, effects of **9a** on cell cycle were analysed. Our lead candidate demonstrated its antiproliferative activity against HeLa cells with an IC_{50} = 3.2 μM, blocking most of the cells in G2/M phase and causing an increased number of cell division defects. Fluorescence microscopy analysis showed a slowed cytokinesis in the same cell line after treatment with **9a**, while high-content confocal microscopy on Hela cells stained for β-tubulin showed tubulin disassembly, allowing us to speculate microtubules as potential target of our lead compound. Structural superimposition of CBSIs in clinical trial and **9a** further suggested the common binding to the colchicine binding site, enlightening a new pattern of electrostatic/hydrophobic interactions. Compound **9a** was also combined with an extrusion pump inhibitor (**SS26**, 1 μM): the co-administration of a microtubule destabilising agent and an EPI determined a more potent antiproliferative activity against four drug-resistant cancer cell lines. All designed and synthesised compounds showed good properties of predicted pharmacokinetics and druglikeness (as reported in SM). In conclusion, we developed a series of small molecules as new MDAs; among them, candidate **9a** showed the best overall activity. Future investigations will be focused on exploring more in depth its pharmacokinetic and pharmacodynamic features, paying particular attention to the intimate interaction between tubulin and **9a**.

5. Experimental Section

*5.1. N-(3,4-difluorophenyl)acetamide (**2**)*

Acetic anhydride (1 ml) was added dropwise to 3,4-difluoroaniline (**1**) (1 g, 0.8 ml, 7.8 mmol,) in an ice-bath (10 min). The white solid was filtrated, washed to reach neutral pH, then dried. $C_8H_7F_2NO$, MW: 171.14; 80% yield (1.1 g, 6.4 mmol), m.p. 107.3-109.4 °C; R_f 0.10. ^{1}H-NMR (DMSO-d_6): δ 10.16 (1H, s, NH), 7.77 (1H, ddd, $^1J_{H\text{-}F}$= 13.2 Hz, $^2J_{meta}$= 7.6 Hz, $^3J_{meta}$= 2.4 Hz, H-2), 7.36 (1H, dd, $^1J_{H\text{-}F}$= 19.3 Hz, $^2J_{meta}$= 9.2 Hz, H-5), 7.25 (1H, wm, H-6), 2.04 (3H, s, CH_3). ^{13}C-NMR (DMSO-d_6): δ 168.51 (C=O), 148.84 (C, dd, $^1J_{C\text{-}F}$= 242 Hz, $^2J_{C\text{-}F}$= 13 Hz, C-F), 144.99 (C, dd, $^1J_{C\text{-}F}$= 240 Hz, $^2J_{C\text{-}F}$= 13 Hz, C-F), 136.31 (C-N), 117.32 (CH), 115.11 (C, d, $J_{C\text{-}F}$= 8 Hz, CH-CF), 107.85 (C, d, $J_{C\text{-}F}$= 22 Hz, CH-CF), 23.86 (CH_3). ESI-MS (*m/z*): calcd for $C_8H_7F_2NO$ 172.05685, found 172.05676 [M + H]$^+$.

*5.2. N-(4,5-difluoro-2-nitrophenyl)acetamide (**3**)*

Compound **2** (1 g, 6.0 mmol) was dissolved in concentrated H_2SO_4 ($H_2SO_{4\ conc}$) in an ice-bath under magnetic stirring. A solution of KNO_3 (1.22 g, 12.0 mmol) in $H_2SO_{4\ conc}$ (3.26 ml) was added dropwise. The solution was brought to r.t. and stirred for 2 h. Next, the reaction was quenched with ice. The obtained precipitate was filtered off and washed with water to reach neutral pH. Pale-yellow solid; $C_8H_6F_2N_2O_3$, MW: 216.14; 79% yield (1 g, 4.6 mmol); m.p. 101.4-102.5 °C; R_f 0.60. ^{1}H-NMR (DMSO-d_6): δ 10.33 (1H, s, NH), 8.22 (1H, t, $^1J_{H\text{-}F}$= 8.8 Hz, H-5), 7.83 (1H, dd, $^1J_{H\text{-}F}$= 11.2 Hz, $^2J_{H\text{-}F}$= 7.6 Hz, H-2), 2.09 (3H, s, CH_3). ^{13}C-NMR (DMSO-d_6): δ 168.82 (C=O), 151.90 (C, dd, $^1J_{C\text{-}F}$= 253

Hz, $^{2}J_{C\text{-}F}$= 13 Hz, C-F), 145.04 (C, dd, $^{1}J_{C\text{-}F}$= 246 Hz, $^{2}J_{C\text{-}F}$= 14 Hz, C-F), 137.45 (C-N), 129.55 (CH), 114.89 (C, d, $J_{C\text{-}F}$= 10 Hz, CH-CF), 113.43 (C, d, $J_{C\text{-}F}$= 22 Hz, CH-CF), 23.39 (CH_3). ESI-MS *m/z* calcd for $C_8H_6F_2N_2O_3$ 217.10478, found 217.04193 $[M + H]^+$.

*5.3. 4,5-difluoro-2-nitroaniline (**4**)*

Intermediate **3** (1 g, 4.6 mmol) was dissolved in $H_2SO_{4\ conc}$ (10 ml) under reflux (2 h). Next, the reaction was quenched with ice. A precipitate was obtained, then filtered off and washed with water to reach pH. Yellow solid; $C_6H_4F_2N_2O_2$, MW: 174.11; 61% yield (1.0 g, 5.7 mmol); m.p. 95.6-105.5 °C; R_f 0.53. ^{1}H-NMR (DMSO-d_6): δ 7.99 (1H, dd, $^{1}J_{H\text{-}F}$= 11.0 Hz, $^{2}J_{H\text{-}F}$= 8.4 Hz, H-5), 7.56 (2H, s, NH_2), 6.96 (1H, dd, $^{1}J_{H\text{-}F}$= 12.8 Hz, $^{2}J_{H\text{-}F}$= 7.2 Hz, H-2). ^{13}C-NMR (DMSO-d_6): δ 154.67 (C, dd, $^{1}J_{C\text{-}F}$= 126 Hz, $^{2}J_{C\text{-}F}$= 15 Hz, C-F), 144.63 (C, d, $J_{C\text{-}F}$= 12 Hz, C), 139.89 (C-F), 125.06 (C-NH_2), 110.93 (CH-CF), 105.41 (C, d, $J_{C\text{-}F}$= 21 Hz, CH-CF). ESI-MS *m/z* calcd for $C_6H_4F_2N_2O_2$ 175.03136, found 174.95352 $[M + H]^+$.

*5.4. 4,5-difluorobenzene-1,2-diamine (**5**)*

Compound **4** (2 g, 11.5 mol) was dissolved in ethanol (200 ml). Pd/C (0.20 g, 10 % w/w) was added. The hydrogenation was performed with the shaking hydrogenation reactor (open tank, 1.5 h). The Pd/C was filtered off and the solution was concentrated in vacuo to obtain a brown oil, which was purified via flash chromatography with DE; Brown solid; $C_6H_6F_2N_2$, MW: 144.12; 98% yield (1.62 g, 11.2 mmol); m.p. 111.6-117.2 °C; R_f 0.10. ^{1}H-NMR (DMSO-d_6): δ 7.04 (2H, t, $^{1}J_{H\text{-}F}$= 10.4 Hz, H-2,5), 5.33 (4H, s, $2NH_2$). ^{13}C-NMR (DMSO-d_6): δ 141.14 (2C, dd, $^{1}J_{C\text{-}F}$= 231 Hz, $^{2}J_{C\text{-}F}$= 15Hz, C-F), 131.46 (2C-NH_2), 102.34-101.71 (2C, m, CH-F). ESI-MS *m/z* calcd for $C_6H_6F_2N_2$ 145.05718, found 145.05730 $[M + H]^+$.

*5.5. 5,6-difluoro-1H-benzo[d][1,2,3]triazole (**6**)*

Compound **5** (1.65 g, 11.0 mmol) was dissolved in HCl 2 N (114 ml) in an ice-bath. An aqueous solution of $NaNO_2$ (1.63 g, 0.3 mol) was added dropwise. The solution was brought to r.t., then extracted with DE. Yellow solid; $C_6H_3F_2N_3$, MW: 155.11; 43% yield (0.8 g, 5.0 mmol); m.p. 179-181 °C; R_f 0.16. Spectra correspondent to lit. [59] δ ESI-MS *m/z* calcd for $C_6H_4F_2N_4$ 154.02113, found 154.02127 $[M - H]^-$.

*5.6. Synthesis and characterisation of the intermediates 2-(5,6-difluoro-1H-benzo[d][1,2,3]triazol-1-yl)acetonitrile (**7a**) and 2-(5,6-difluoro-1H-benzo[d][1,2,3]triazol-1-yl)acetonitrile (**7b**)*

Compound (**6**) (2.4 g, 15.3 mmol), KOH (0.95 g, 16.9 mmol) and chloroacetonitrile (0.9 ml, 1.0 g, 13.8 mmol) were dissolved in acetonitrile (20 ml), at 80 °C under reflux overnight. The solution was concentrated in vacuo and purified via flash chromatography (PS/EA 8/2). These reaction conditions have a good influence on the selective formation of the 1-isomer compared to the 2-isomer (ratio 3:1). (**7a**) Orange solid; $C_8H_4F_2N_4$, MW: 194.14; 9% yield (0.26 g, 1.3 mmol); m.p. 97.3-99.1 °C; R_f 0.20. ^{1}H-NMR (DMSO-d_6): δ 8.17 (2H, t, $^{1}J_{H\text{-}F}$= 8.8 Hz, H-4,7), 6.28 (2H, s, CH_2). ^{13}C-NMR (DMSO-d_6): δ 150.85 (2C, d, $^{1}J_{C\text{-}F}$= 249.2 Hz, $^{2}J_{C\text{-}F}$= 19.3 Hz, C-F), 140.13 (2C, t, $^{1}J_{C\text{-}F}$= 6.0 Hz, C=N), 114.12 (C≡N), 104.30 (2C, m, CH-CF), 44.0 (CH_2). ESI-MS *m/z* calcd for $C_8H_4F_2N_4$ 193.03203, found 193.03246 $[M - H]^-$. (**7b)** Yellow solid; $C_8H_4F_2N_4$, MW: 194.14; 33% yield (0.98 g, 5.0 mmol); m.p. 129.2-131.3 °C; R_f 0.18 (PS/EA 7/3). ^{1}H-NMR (DMSO-d_6): δ 8.29 (1H, dd, $^{1}J_{H\text{-}F}$= 10.0 Hz, $^{2}J_{H\text{-}F}$= 7.2 Hz, H-4), 8.21 (1H, dd, $^{1}J_{H\text{-}F}$= 9.6 Hz, $^{2}J_{H\text{-}F}$= 6.8 Hz, H-7), 6.14 (2H, s, CH_2). ^{13}C-NMR (DMSO-

d6): δ 150.87 (1C, dd, $^1J_{C\text{-}F}$= 240.6 Hz, $^2J_{C\text{-}F}$= 16.8 Hz, C-F), 148.41 (1C, dd, $^1J_{C\text{-}F}$= 233.5 Hz, $^2J_{C\text{-}F}$= 22.0 Hz, C-F), 140.32 (1C, d, $^1J_{C\text{-}F}$= 11.0 Hz, C=N), 128.79 (1C, d, $^1J_{C\text{-}F}$= 12.0 Hz, C=N), 114.76 (C≡N), 106.65 (1C, dd, $^1J_{C\text{-}F}$= 20.4 Hz, CH), 98.53 (1C, d, $^1J_{C\text{-}F}$= 25.0 Hz, CH), 36.01 (CH_2). ESI-MS *m/z* calcd for $C_6H_4F_2N_4$ 193.03203, found 193.03242 $[M - H]^-$.

*5.7. General procedure for final compounds **9a-j**, **10e**, **11a,b** and **13d,j**.*

Compounds **9a-j** and **10e** were obtained from **7b** and **8a-j** (ratio 1:1), **11a,b** from **7a** and **8a,b** (ratio 1:1) and **13d,j** from **12a** and **8d,j** (ratio 1:1). Triethylamine (TEA, ratio 1:1+20%) was used as a base for products **9a-c,e-j**, **10e** and **11a,b**, in toluene as a solvent at 110 °C. DIMCARB (ratio 1:1+20%) was used as a catalyst for products **9d** and **13d**, in acetonitrile at 60 °C. Piperidine was used as a base for product **13j**, in acetonitrile at 60 °C. Some of the final compounds were (1) filtrated and crystallised from EtOH, (2) some were worked-up through liquid chromatography.

*5.8. (E)-2-(5,6-difluoro-1H-benzo[d][1,2,3]triazol-1-yl)-3-(p-tolyl)acrylonitrile (**9a**)*

Work-up procedure (2): PS/EA 9.5/0.5. White solid; $C_{16}H_{10}F_2N_4$, MW: 296,28; 45% yield (0.24 g, 0.8 mmol); m.p. 121.4-122.5 °C; R_f 0.72. ^{1}H-NMR (DMSO-*d6*): δ 8.50 (1H, dd, $^1J_{H\text{-}F}$= 10.0 Hz, $^2J_{H\text{-}F}$= 7.2 Hz, H-4'), 8.38 (1H, dd, $^1J_{H\text{-}F}$= 9.8 Hz, $^2J_{H\text{-}F}$= 7.2 Hz, H-7'), 8.28 (1H, s, =CH), 7.98 (2H, d, $^1J_{H\text{-}H}$= 8.0 Hz, H-2",6"), 7.51 (2H, d, $^1J_{H\text{-}H}$= 8.4 Hz, H-3",5"), 2.48 (3H, s, CH_3). ^{13}C-NMR (DMSO-*d6*): δ 151.34 (1C, dd, $^1J_{H\text{-}F}$= 241.2 Hz, $^2J_{H\text{-}F}$= 16.6 Hz, C-F), 148.63 (1C, dd, $^1J_{H\text{-}F}$= 244.5 Hz, $^2J_{H\text{-}F}$= 16.2 Hz, C-F), 142.61 (C-CH_3), 142.43 (=CH), 140.6 (1C, d, $J_{H\text{-}F}$= 10.4 Hz, C=N), 129.80 (4C, m, CH), 128.08 (1C, d, $J_{H\text{-}F}$= 12.0 Hz, C=N), 127.68 (C), 114.15 (C≡N), 107.04 (1C, d, $^1J_{C\text{-}F}$= 20.8 Hz, CH-CF), 104.71 (C=CH), 99.65 (1C, d, $^1J_{C\text{-}F}$= 24.6 Hz, CH-CF), 21.15 (CH_3). ESI-MS *m/z* calcd for $C_{16}H_{10}F_2N_4$ 297.09463, 298.09798, found 297.09467, 298.09808 $[M + H]^+$.

*5.9. (E)-2-(5,6-difluoro-1H-benzo[d][1,2,3]triazol-1-yl)-3-(4-methoxyphenyl)acrylonitrile (**9b**)*

Work-up procedure (1). Brown solid; $C_{16}H_{10}F_2N_4O$, MW: 312,28; 37% yield (0.18 g; 0.6 mmol); m.p. 102.8-103.4 °C; R_f 0.48. ^{1}H-NMR (DMSO-*d6*): δ 8.43 (1H, dd, $^1J_{H\text{-}F}$= 9.8 Hz, $^2J_{H\text{-}F}$= 7.2 Hz, H-4'), 8.29 (1H, dd, $^1J_{H\text{-}F}$= 9.4 Hz, $^2J_{H\text{-}F}$= 7.2 Hz, H-7'), 8.18 (1H, s, =CH), 8.02 (2H, d, $J_{H\text{-}H}$= 8.8 Hz, H-2",6"), 7.21 (2H, d, $J_{H\text{-}H}$= 8.8 Hz, H-3",5"), 3.89 (3H, s, OCH_3). ^{13}C-NMR (DMSO-*d6*): δ 162.42 (C-OCH_3), 151.30 (1C, dd, $^1J_{H\text{-}F}$= 250.0 Hz, $^2J_{H\text{-}F}$= 16.7 Hz, C-F), 148.62 (1C, dd, $^1J_{H\text{-}F}$= 244.0 Hz, $^2J_{H\text{-}F}$= 16.3 Hz, C-F), 142.79 (=CH), 140.52 (1C, d, $J_{H\text{-}F}$= 10.4 Hz, C=N), 131.97 (2CH), 128.20 (1C, d, $J_{H\text{-}F}$= 12.3 Hz, C=N), 122.71 (C), 114.85 (2CH), 114.57 (C≡N), 106.99 (1C, d, $^1J_{C\text{-}F}$= 20.9 Hz, CH-CF), 102.57 (C=CH), 99.52 (1C, d, $^1J_{C\text{-}F}$= 24.6 Hz, CH-CF), 55.58 (CH_3). ESI-MS *m/z* calcd for $C_{16}H_{10}F_2N_4O$ 313.08954, 314.09290, found 313.08945, 314.09280 $[M + H]^+$.

*5.10. (E)-2-(5,6-difluoro-1H-benzo[d][1,2,3]triazol-1-yl)-3-(2,3,4-trimethoxyphenyl)acrylonitrile (**9c**)*

Work-up procedure (2): PS/EA 9/1. Yellow solid; $C_{18}H_{14}F_2N_4O_3$, MW: 344,32; 21% yield (0.1 g, 0.3 mmol); m.p. 119.3-120.6 °C; R_f 0.43. ^{1}H-NMR (DMSO-*d6*): δ 8.44 (1H, dd, $^1J_{H\text{-}F}$= 9.6 Hz, $^2J_{H\text{-}F}$= 7.2 Hz, H-4'), 8.21 (1H, dd, $^1J_{H\text{-}F}$= 9.6 Hz, $^2J_{H\text{-}F}$= 6.8 Hz, H-7'), 8.11 (1H, s, C=CH), 7.94 (1H, d, $J_{H\text{-}H}$= 8.8 Hz, H-6"), 7.13 (1H, d, $J_{H\text{-}H}$= 8.8 Hz, H-5"), 3.94 (3H, s, OCH_3), 3.90 (3H, s, OCH_3), 3.81 (3H, s, OCH_3). ^{13}C-NMR (DMSO-*d6*): δ 156.99 (C-OCH_3), 153.14 (2C-OCH_3), 141.52 (C), 140.32 (CF), 138.04 (CH), 128.44 (CF), 123.56 (CH), 116.76 (2C), 114.30 (C≡N), 108.47 (CH), 107.06 (1C, d, $^1J_{C\text{-}F}$= 21.6 Hz, CH-CF), 104.09 (C=CH), 99.20 (1C, d, $^1J_{C\text{-}F}$= 24.7 Hz, CH-CF), 61.82 (OCH_3), 60.43

(OCH_3), 56.19 (OCH_3). ESI-MS *m/z* calcd for $C_{18}H_{14}F_2N_4O_3$ 373.11067, 374.11403, found 373.11124, 374.11432 $[M + H]^+$; calcd 395.092962, 396.09597, found 395.09296, 396.09625 $[M + Na]^+$; calcd 411.06656, found 411.06683 $[M + K]^+$.

*5.11. (E)-2-(5,6-difluoro-1H-benzo[d][1,2,3]triazol-1-yl)-3-(4-hydroxyphenyl)acrylonitrile (**9d**)*

Work-up procedure (1). Yellow solid; $C_{15}H_8F_2N_5O$, MW: 298.25; 29% yield (0.12 g, 0.40 mmol); m.p. 178.4-180,6 °C; R_f 0.18. ^{1}H-NMR (DMSO-d_6): δ 10.59 (1H, s, OH), 8.41 (1H, dd, $^1J_{H-F}$= 9.6 Hz, $^2J_{H-F}$= 7.2 Hz, H-4'), 8.25 (1H, dd, $^1J_{H-F}$= 9.0 Hz, $^2J_{H-F}$= 6.8 Hz, H-7'), 8.09 (1H, s, =CH), 7.92 (2H, d, J_{H-H}= 8.0 Hz, H-2",6"), 7.0 (2H, d, J_{H-H}= 8.0 Hz, H-3",5"). ^{13}C-NMR (DMSO-d_6): δ 161.54 (C-OH), 151.28 (1C, dd, $^1J_{H-F}$= 249.0 Hz, $^2J_{H-F}$= 17.0 Hz, C-F), 148.59 (1C, dd, $^1J_{H-F}$= 244.5 Hz, $^2J_{H-F}$= 17.0 Hz, C-F), 143.62 (CH=C), 140.46 (1C, d, J_{H-F}= 10.0 Hz, C=N), 132.31 (2CH), 128.30 (1C, d, J_{H-F}= 12.0 Hz, C=N), 121.11 (C), 116.23 (2CH), 114.81 (C≡N), 106.94 (1C, d, $^1J_{C-F}$= 21.0 Hz, CH-CF), 101.17 (C=C), 99.39 (1C, d, $^1J_{C-F}$= 25.0 Hz, CH-CF). ESI-MS *m/z* calcd for $C_{15}H_8F_2N_5O$ 297.05824, 298.06160, 299.06495, found 297.05939, 298.06268, 299.06622 $[M - H]^-$.

*5.12. (E)-2-(5,6-difluoro-1H-benzo[d][1,2,3]triazol-1-yl)-3-(4-nitrophenyl)acrylonitrile (**9e**)*

Work-up procedure (2): PS/EA 8/2. Yellow powder; $C_{15}H_7F_2N_5O_2$, MW: 327.25; 24% yield (0.11 g, 0.3 mmol); m.p. 151.1-152.6 °C; R_f 0.46. ^{1}H-NMR (DMSO-d_6): δ 8.51-8.42 (2H, m, H-4',7'), 8.48 (2H, d, J_{H-H}= 8.8 Hz, H-3",5"), 8.43 (1H, s, =CH), 8.23 (2H, d, J_{H-H}= 8.4 Hz, H-2",6"). ^{13}C-NMR (DMSO-d_6): δ 151.47 (1C, dd, $^1J_{H-F}$= 249.5 Hz, $^2J_{H-F}$= 17.0 Hz, C-F), 148.70 (1C, dd, $^1J_{H-F}$= 245.0 Hz, $^2J_{H-F}$= 16.0 Hz, C-F), 148.48 (C-NO_2), 140.84 (1C, d, J_{H-F}= 10.0 Hz, C=N), 137.61 (=CH), 137.03 (C), 130.79 (2CH), 127.71 (1C, d, J_{H-F}= 12.0 Hz, C=N), 124.13 (2CH), 113.15 (C≡N), 109.56 (C=CH), 107.23 (1C, d, $^1J_{C-F}$= 20.0 Hz, CH-CF), 100.17 (1C, d, $^1J_{C-F}$= 24.0 Hz, CH-CF). ESI-MS *m/z* calcd for $C_{15}H_7F_2N_5O_2$ 328.06406, found 328.06406 $[M + H]^+$.

*5.13. (E)-2-(5,6-difluoro-1H-benzo[d][1,2,3]triazol-1-yl)-3-(4-fluorophenyl)acrylonitrile (**9f**)*

Work-up procedure (1). Light brown solid; $C_{15}H_7F_3N_4$, MW: 300,24; 19% yield (0.06 g, 0.2 mmol); m.p. 135.3-136.4 °C; R_f 0.67. ^{1}H-NMR (DMSO-d_6): δ 8.46 (1H, dd, $^1J_{H-F}$= 9.8 Hz, $^2J_{H-F}$= 7.2 Hz, H-4'), 8.35 (1H, dd, $^1J_{H-F}$= 10.0 Hz, $^2J_{H-F}$= 6.8 Hz, H-7'), 8.28 (1H, s, =CH), 8.10 (2H, dd, J_{H-H}= 8.4 Hz e J_{H-H}= 5.2 Hz, H-2",6"), 7.51 (2H, t, H-3",5"). ^{13}C-NMR (DMSO-d_6): δ 165.11 (C), 162,40 (C), 151.39 (1C, dd, $^1J_{H-F}$= 251.3 Hz, $^2J_{H-F}$= 20.0 Hz, C-F), 148.65 (1C, dd, $^1J_{H-F}$= 245.1 Hz, $^2J_{H-F}$= 16.1 Hz, C-F), 140.80 (=CH), 140.64 (1C, d, J_{H-F}= 10.3 Hz, C=N), 132.38 (2C, d, $^1J_{C-F}$= 9.1 Hz, CH-CF), 128.01 (1C, d, J_{H-F}= 12.4 Hz, C=N), 127.16 (C), 116.47 (2C, d, $^1J_{C-F}$= 22.1 Hz, CH-CF), 113.88 (C≡N), 107.09 (1C, d, $^1J_{C-F}$= 20.7 Hz, CH-CF), 99.77 (1C, d, $^1J_{C-F}$= 24.9 Hz, CH-CF). ESI-MS *m/z* calcd for $C_{15}H_7F_3N_4$ 301.06956, 302.07291, found 301.06961, 302.07288 $[M + H]^+$.

*5.14. (E)-3-(4-chlorophenyl)-2-(5,6-difluoro-1H-benzo[d][1,2,3]triazol-1-yl)acrylonitrile (**9g**)*

Work-up procedure (2): PS/EA 9/1. Light brown solid; $C_{15}H_7ClF_2N_4$, MW: 316.70; 34% yield (0.27 g, 0.9 mmol); m.p. 147.3-149.7 °C; R_f 0.50. ^{1}H-NMR (DMSO-d_6): δ 8.46 (1H, dd, $^1J_{H-F}$= 9.6 Hz, $^2J_{H-F}$= 7.2 Hz, H-4'), 8.36 (1H, dd, $^1J_{H-F}$= 9.6 Hz, $^2J_{H-F}$= 6.8 Hz, H-7'), 8.28 (1H, s, =CH), 8.02 (2H, d, J_{H-H}= 8.8 Hz, H-2",6"), 7.73 (2H, d, J_{H-H}= 8.8 Hz, H-3",5"). ^{13}C-NMR (DMSO-d_6): δ 151.39 (1C, dd,

$^{1}J_{H\text{-}F}$= 249.0 Hz, $^{2}J_{H\text{-}F}$= 16.0 Hz, C-F), 148.69 (1C, dd, $^{1}J_{H\text{-}F}$= 245.0 Hz, $^{2}J_{H\text{-}F}$= 16.0 Hz, C-F), 140.69 (1C, d, $J_{H\text{-}F}$= 11.0 Hz, C=N), 140.13 (=CH), 136.49 (C), 131.38 (2CH), 129.46 (C-Cl), 129.33 (2CH), 127.91 (1C, d, $J_{H\text{-}F}$= 12.0 Hz, C=N), 113.69 (C≡N), 107.11 (1C, d, $^{1}J_{C\text{-}F}$= 20.0 Hz, CH-CF), 106.63 (C=CH), 99.85 (1C, d, $^{1}J_{C\text{-}F}$= 24.0 Hz, CH-CF). ESI-MS *m/z* calcd for $C_{15}H_7ClF_2N_4$ 317.04001, found 317.04178 $[M + H]^+$.

*5.15. (E)-3-(4-bromophenyl)-2-(5,6-difluoro-1H-benzo[d][1,2,3]triazol-1-yl)acrylonitrile (**9h**)*

Work-up procedure (2): PS/DE 8/2. White powder; $C_{15}H_7BrF_2N_4$, MW: 361.15; 47% yield (0.35 g, 1.0 mmol); m.p. 150.0-151.6 °C; R_f 0.3. ^{1}H-NMR (DMSO-d_6): δ 8.46 (1H, dd, $^{1}J_{H\text{-}F}$= 9.8 Hz, $^{2}J_{H\text{-}F}$= 7.6 Hz, H-4'), 8.37 (1H, dd, $^{1}J_{H\text{-}F}$= 9.6 Hz, $^{2}J_{H\text{-}F}$= 6.8 Hz, H-7'), 8.26 (1H, s, =CH), 7.95 (2H, d, $J_{H\text{-}H}$= 8.8 Hz, H-2",6"), 7.87 (2H, d, $J_{H\text{-}H}$= 8.4 Hz, H-3",5"). ^{13}C-NMR (DMSO-d_6): δ 151.41 (1C, dd, $^{1}J_{H\text{-}F}$= 250.0 Hz, $^{2}J_{H\text{-}F}$= 16.4 Hz, C-F), 148.67 (1C, dd, $^{1}J_{H\text{-}F}$= 245.0 Hz, $^{2}J_{H\text{-}F}$= 16.2 Hz, C-F), 140.69 (1C, d, $J_{H\text{-}F}$= 10.2 Hz, C=N), 140.13 (=CH), 132.20 (2CH), 131.43 (2CH), 129.75 (C), 127.85 (1C, d, $J_{H\text{-}F}$= 12.4 Hz, C=N), 125.43 (C-Br), 113.59 (C≡N), 107.01 (1C, d, $^{1}J_{C\text{-}F}$= 19.4 Hz, CH-CF), 106.67 (C=C), 99.72 (1C, d, $^{1}J_{C\text{-}F}$= 24.8 Hz, CH-CF). ESI-MS *m/z* $[M + H]^+$.

*5.16. (E)-3-(benzo[d][1,3]dioxol-4-yl)-2-(5,6-difluoro-1H-benzo[d][1,2,3]triazol-1-yl)acrylonitrile (**9i**)*

Work-up procedure (1). Yellow solid; $C_6H_8F_2N_4O_2$, MW: 326,26; 28% yield (0.13 g, 0.4 mmol); m.p. 164.6-165.2 °C; R_f 0,41. ^{1}H-NMR (DMSO-d_6): δ 8.44 (1H, dd, $^{1}J_{H\text{-}F}$= 9.6 Hz, $^{2}J_{H\text{-}F}$= 7.2 Hz, H-4'), 8.28 (1H, dd, $^{1}J_{H\text{-}F}$= 9.6 Hz, $^{2}J_{H\text{-}F}$= 6.8 Hz, H-7'), 8.15 (1H, s, =CH), 7.62 (1H, d, $J_{H\text{-}H}$= 1.6 Hz, H-2"), 7.56 (1H, dd, $J_{H\text{-}H}$= 8.4 Hz e J= 1.6 Hz, H-6"), 7.20 (1H, d, $J_{H\text{-}H}$= 8.4 Hz, H-5"), 6.21 (2H, s, CH_2). ^{13}C-NMR (DMSO-d_6): δ 151.76 (1C, dd, $^{1}J_{H\text{-}F}$= 249.6 Hz, $^{2}J_{H\text{-}F}$= 16.6 Hz, C-F), 151.29 (C-O), 149.10 (1C, dd, $^{1}J_{H\text{-}F}$= 245.0 Hz, $^{2}J_{H\text{-}F}$= 16.2 Hz, C-F), 148.42 (C-O), 146.92 (=CH), 142.92 (CH), 141.06 (1C, d, $J_{H\text{-}F}$= 10.4 Hz, C=N), 128.59 (1C, d, $J_{H\text{-}F}$= 12.4 Hz, C=N), 127.52 (CH), 124.70 (C), 114.86 (C≡N), 109.49 (CH), 108.44 (CH), 107.46 (2CH, d, $^{1}J_{C\text{-}F}$= 28.0 Hz, CH-CF), 103.68 (C=CH), 102.76 (O-CH_2-O), 99.96 (2CH, d, $^{1}J_{C\text{-}F}$= 24.8 Hz, CH-CF). ESI-MS *m/z* calcd for $C_{16}H_8F_2N_4O_2$ 327.06881, 328.07216, found 327.06906, 328.07233 $[M + H]^+$.

*5.17. (E)-2-(5,6-difluoro-1H-benzo[d][1,2,3]triazol-1-yl)-3-(isoquinolin-5-yl)acrylonitrile (**9j**)*

Work-up procedure (1). Light brown solid; $C_{18}H_9F_2N_5$, MW: 333.30; 33% yield (0.2 g, 0.6 mmol); m.p. 109.4-111.5 °C; R_f 0.10. ^{1}H-NMR (DMSO-d_6): δ 9.47 (1H, s, H-1"), 8.91 (1H, s, =CH), 8.64 (1H, d, $J_{H\text{-}H}$= 6 Hz, H-3"), 8.49 (1H, d, $J_{H\text{-}H}$= 7.2 Hz, H-8"), 8.44 (2H, m, H-4',7'), 8.39 (1H, d, $J_{H\text{-}H}$= 8.4 Hz, H-6"), 8.12 (1H, d, $J_{H\text{-}H}$= 6.0 Hz, H-4"), 7.93 (1H, t, $J_{H\text{-}H}$= 7.8 Hz, H-7"). ^{13}C-NMR (DMSO-d_6): δ 153.05 (CH), 151.43 (1C, dd, $^{1}J_{H\text{-}F}$= 249.0 Hz, $^{2}J_{H\text{-}F}$= 16.0 Hz, C-F), 148.68 (1C, dd, $^{1}J_{H\text{-}F}$= 245.0 Hz, $^{2}J_{H\text{-}F}$= 16.0 Hz, C-F), 144.03 (CH), 140.73 (1C, d, $J_{c\text{-}F}$= 11.0 Hz, C=N), 138.08 (CH), 133.64 (C=CH), 131.45 (CH), 131.23 (CH), 128.18 (1C, d, $J_{c\text{-}F}$= 13.0 Hz, C=N), 128.06 (C), 127.50 (C), 127.17 (=CH), 117.25 (CH), 113.42 (C≡N), 109.82 (C), 107.07 (2CH, d, $^{1}J_{C\text{-}F}$= 21.0 Hz, CH-CF), 100.16 (2CH, d, $^{1}J_{C\text{-}F}$= 25.0 Hz, CH-CF). ESI-MS *m/z* calcd for $C_{18}H_9F_2N_5$ 334.08988, 335.09323, 336.09659, found 334.09045, 335.09366, 336.09689 $[M + H]^+$.

*5.18. (Z)-2-(5,6-difluoro-1H-benzo[d][1,2,3]triazol-1-yl)-3-(4-nitrophenyl)acrylonitrile (**10e**)*

Work-up procedure (1). Red solid; $C_{15}H_7F_2N_5O_2$, MW: 327.25; 26% yield (0.12 g, 0.4 mmol); m.p. 179.3-181.2 °C; R_f 0,68. ^{1}H-NMR (DMSO-d_6): δ 8.53 (1H, dd, $^1J_{H\text{-}F}$= 10.0 Hz, $^2J_{H\text{-}F}$= 7.2 Hz, H-4'), 8.32 (2H, d, $J_{H\text{-}H}$= 8.8 Hz, H-3",5"), 7.74 (1H, dd, $^1J_{H\text{-}F}$= 9.6 Hz, $^2J_{H\text{-}F}$= 6.8 Hz, H-7'), 7.69 (2H, d, $J_{H\text{-}H}$= 8.8 Hz, H-2",6"), 7.27 (1H, s, =CH). ^{13}C-NMR (DMSO-d_6): δ 151.34 (1C, dd, $^1J_{C\text{-}F}$= 250.5 Hz, $^2J_{C\text{-}F}$= 16.0 Hz, C-F), 149.45 (C-NO_2), 148.70 (1C, dd, $^1J_{C\text{-}F}$= 227.5 Hz, $^2J_{C\text{-}F}$= 16.0 Hz, C-F), 147.63 (C), 140.59 (1C, d, $J_{H\text{-}F}$= 10.0 Hz, C=N), 137.20 (C=CH), 129.19 (2CH), 124.18 (1C, d, $J_{H\text{-}F}$= 17.0 Hz, C=N), 124.26 (2CH), 114.83 (C≡N), 107.43 (2CH, d, $^1J_{C\text{-}F}$= 20.0 Hz, CH-CF), 99.77 (1C, d, $^1J_{C\text{-}F}$= 25.0 Hz, CH-CF), 99.64 (=CH). ESI-MS *m/z* calcd for $C_{18}H_9F_2N_5$ 311.06467, found 311.25558 $[M + H]^+$.

*5.19. (E)-2-(5,6-difluoro-2H-benzo[d][1,2,3]triazol-2-yl)-3-(p-tolyl)acrylonitrile (**11a**)*

Work-up procedure (1). Yellow solid; $C_{16}H_{10}F_2N_4$, MW: 296,28; 42% yield (0.16 g, 0.5 mmol); m.p. 158.1-160.5 °C; R_f 0,83. ^{1}H-NMR (DMSO-d_6): δ 8.66 (1H, s, =CH), 8.23 (2H, t, $^1J_{H\text{-}H}$= 8.8 Hz, H-4',7'), 7.96 (2H, d, $J_{H\text{-}H}$= 8.0 Hz, H-2",6"), 7.44 (2H, d, $J_{H\text{-}H}$= 8.0 Hz, H-3",5"), 2.42 (3H, s, CH_3). ^{13}C-NMR (DMSO-d_6): δ 151.39 (2C, dd, $^1J_{C\text{-}F}$= 250.5 Hz, $^2J_{C\text{-}F}$= 19.0 Hz, C-F), 142.87 (2C, t, $^1J_{C\text{-}F}$= 7.0 Hz, C=N), 138.24 (C=CH), 130.00 (2CH), 129.96 (2CH), 127.27 (C), 113.08 (C≡N), 110.45 (C=CH), 104.33 (2CH, m, CH-CF), 21.23 (CH_3). ESI-MS *m/z* calcd for $C_{16}H_{10}F_2N_4$ 297.09463, found 297.09482 $[M + H]^+$.

*5.20. (E)-2-(5,6-difluoro-2H-benzo[d][1,2,3]triazol-2-yl)-3-(4-methoxyphenyl)acrylonitrile (**11b**)*

Work-up procedure (1). Brown solid; $C_{16}H_{10}F_2N_4O$, MW: 312,28; 39% yield (0.17 g, mmol); m.p. 148.6-149.3 °C; R_f 0,43. ^{1}H-NMR (DMSO-d_6): δ 8.62 (1H, s, =CH), 8.21 (2H, t, $^1J_{H\text{-}H}$= 8.8 Hz, H-4',7'), 8.06 (2H, d, $J_{H\text{-}H}$= 8.8 Hz, H-2",6"), 7.18 (2H, d, $J_{H\text{-}H}$= 8.8 Hz, H-3",5"), 3.88 (3H, s, OCH_3). ^{13}C-NMR (DMSO-d_6): δ 162.52 (C-OCH_3), 151.27 (2C, dd, $^1J_{C\text{-}F}$= 250.5 Hz, $^2J_{C\text{-}F}$= 20.0 Hz, C-F), 140.37 (2C, t, $^1J_{C\text{-}F}$= 6.0 Hz, C=N), 138.07 (C=CH), 132.23 (2CH), 122.32 (C), 114.97 (2CH), 113.43 (C≡N), 108.68 (C=CH), 104.24 (2CH, m, CH-CF), 55.64 (CH_3). ESI-MS *m/z* calcd for $C_{16}H_{10}F_2N_4O$ 313.08954, found 313.08975 $[M + H]^+$.

*5.21. (E)-2-(1H-benzo[d][1,2,3]triazol-1-yl)-3-(4-hydroxyphenyl)acrylonitrile (**13d**)*

Work-up procedure (2): $CHCl_3$/CH_3OH 9.9/0.1. Yellow solid; $C_{15}H_{10}N_4O$, MW: 262.27; 28% yield (0.2 g, 0.8 mmol); m.p. 115.4-116.5 °C; R_f 0.38. ^{1}H-NMR (DMSO-d_6): δ 8.22 (2H, d, $^1J_{H\text{-}H}$= 8.4 Hz, H-4'), 8.12 (1H, s, =CH), 7.98 (1H, d, $J_{H\text{-}H}$= 8.4 Hz, H-7'), 7.93 (2H, d, $J_{H\text{-}H}$= 8.4 Hz, H-2",6"), 7.73 (1H, d, $J_{H\text{-}H}$= 7.8 Hz, H-6'), 7.00 (2H, d, $J_{H\text{-}H}$= 8.4 Hz, H-3",5"). ^{13}C-NMR (DMSO-d_6): δ 161.86 (C-OH), 145.71 (C=N), 143.31 (CH), 132.61 (2CH), 132.29 (C=N), 129.63 (CH), 125.68 (CH), 121.75 (C-CH), 120.35 (CH), 116.73 (2CH), 115.39 (C≡N), 111.30 (CH), 102.06 (C). ESI-MS *m/z* calcd for $C_{15}H_{10}N_4O$ 263.09274, found 263.53491 $[M - H]^-$.

*5.22. (E)-2-(1H-benzo[d][1,2,3]triazol-1-yl)-3-(isoquinolin-5-yl)acrylonitrile (**13j**)*

Work-up procedure (1). Brick red-brown powder. $C_{18}H_{11}N_5$, MW: 297.32; 35% yield (0.23 g, 0.8 mmol); m.p. 131.4 – 133.3 °C; R_f 0.04. ^{1}H-NMR (DMSO-d_6): δ 9.47 (1H, s, H-1"), 8.92 (1H, s, =CH), 8.63 (1H, d, $J_{H\text{-}H}$= 5.6 Hz, H-3"), 8.50 (1H, d, $J_{H\text{-}H}$= 7.2 Hz, H-4'), 8.39 (1H, d, $J_{H\text{-}H}$= 8.0 Hz, H-4"), 8.28 (1H, d, $J_{H\text{-}H}$= 8.4 Hz, H-8"), 8.18 (1H, d, $J_{H\text{-}H}$= 8.4 Hz, H-7'), 8.14 (1H, d, $J_{H\text{-}H}$= 6 Hz, H-6"), 7.93 (1H, t, $J_{H\text{-}H}$= 8.0 Hz, H-6'), 7.79 (1H, t, $J_{H\text{-}H}$= 8.0 Hz, H-7"), 7.62 (1H, t, $J_{H\text{-}H}$= 8.0 Hz, H-

5').^{13}C-NMR (DMSO-d_6): δ 153.05 (CH=N isoq), 145.49 (C=N), 144.06 (CH=N isoq), 137.02 (CH), 133.65 (C=CH), 131.62 (C=N), 131.41 (CH), 131.09 (CH), 129.44 (CH), 128.09 (C), 127.60 (C), 127.20 (CH), 125.53 (CH), 119.99 (=CH), 117.20 (CH), 113.53 (CN), 111.51 (CH), 110.34 (C). ESI-MS *m/z* calcd for $C_{15}H_{10}N_4O$, found 263.06778, 264.07114 $[M + H]^+$.

6. Acknowledgments

We thank the National Cancer Institute, Developmental Therapeutics Program, NCI (Bethesda, MD, USA; https://dtp.cancer.gov) as the source of the data from *in vitro* anti-cancer screening. We acknowledge CISUP—Centre for Instrumentation Sharing— Operetta CLS Facility -University of Pisa. We thank Kitos Biotech for *in vitro* **9a**-EPI combination assay. We acknowledge Schrödinger® for the short term free license of Maestro package. F.R. acknowledges MIUR (Ministero dell'Istruzione, dell'Università e della Ricerca) for the PhD grant, and the Erasmus+ program. F.R. thanks Prof. Göran Widmalm and Alessandro Ruda, for the support during his PhD Erasmus+ at the Stockholm University, Sweden.

7. Fundings

This work was supported by "Regione Autonoma della Sardegna" (Sardinia, Italy), by "Legge Regionale 7 agosto 2007:CRP1_574, 22/41 del 2017" [grant number RASSR01499].

8. Author Contributions

Conceptualisation, F.R., R.I., S.P. and A.C.; formal analysis, F.R., R.I., S.S., V.B., L.S., M.A.S. and M.L.; investigation, F.R., R.I., V.B., L.S., M.A.S. and M.L.; resources, A.C.; data curation, F.R., R.I., S.S. V.B., L.S., M.A.S., M.L., L.B. and A.C.; writing/original draft preparation, F.R., R.I.; writing/review and editing, all authors; visualization, F.R., R.I., S.S. and A.C.; supervision, L.B., A.C., funding acquisition, L.B., A.C. All authors have read and agreed to the published version of the manuscript.

9. Conflict of interest

The authors declare that the research was conducted in the absence of any commercial or financial relationships that could be construed as a potential conflict of interest.

10. Appendix A. Supplementary Material reports deeper NMR studies, NCI60 tables, EPI **SS26** activity validation, further association assay results and ADME prediction tables.

11. References

[1] F. Bray, J. Ferlay, I. Soerjomataram, R.L. Siegel, L.A. Torre, A. Jemal, Global cancer statistics 2018: GLOBOCAN estimates of incidence and mortality worldwide for 36 cancers in 185 countries., CA. Cancer J. Clin. 68 (2018) 394–424. https://doi.org/10.3322/caac.21492.

[2] A. Damasceno, Noncommunicable Disease, 2016. https://doi.org/10.1002/9781119097136.part5.

[3] G. Bérubé, How to utilize academic research efforts in cancer drug discovery, Expert Opin. Drug Discov. 14 (2019) 331–334. https://doi.org/10.1080/17460441.2019.1582637.

[4] Y. Imoto, Y. Yoshida, F. Yagisawa, H. Kuroiwa, T. Kuroiwa, The cell cycle, including the mitotic cycle and organelle division cycles, as revealed by cytological observations, J.

Electron Microsc. (Tokyo). 60 (2011) 117–136. https://doi.org/10.1093/jmicro/dfr034.
[5] S. Florian, T.J. Mitchison, Anti-microtubule drugs, Methods Mol. Biol. 1413 (2016) 403–421. https://doi.org/10.1007/978-1-4939-3542-0_25.
[6] G. Chandrasekaran, P. Tátrai, F. Gergely, Hitting the brakes: Targeting microtubule motors in cancer, Br. J. Cancer. 113 (2015) 693–698. https://doi.org/10.1038/bjc.2015.264.
[7] E. Mukhtar, V.M. Adhami, H. Mukhtar, Targeting microtubules by natural agents for cancer therapy, Mol. Cancer Ther. 13 (2014) 275–284. https://doi.org/10.1158/1535-7163.MCT-13-0791.
[8] A. Jordan, J.A. Hadfield, N.J. Lawrence, A.T. McGown, Tubulin as a target for anticancer drugs: Agents which interact with the mitotic spindle, Med. Res. Rev. (1998). https://doi.org/10.1002/(SICI)1098-1128(199807)18:4<259::AID-MED3>3.0.CO;2-U.
[9] R. Kaul, A.L. Risinger, S.L. Mooberry, Microtubule-Targeting Drugs: More than Antimitotics, J. Nat. Prod. (2019). https://doi.org/10.1021/acs.jnatprod.9b00105.
[10] Y.N. Cao, L.L. Zheng, D. Wang, X.X. Liang, F. Gao, X.L. Zhou, Recent advances in microtubule-stabilizing agents, Eur. J. Med. Chem. (2018). https://doi.org/10.1016/j.ejmech.2017.11.062.
[11] S.K. Coulup, G.I. Georg, Revisiting microtubule targeting agents: α-Tubulin and the pironetin binding site as unexplored targets for cancer therapeutics, Bioorg. Med. Chem. Lett. 29 (2019) 1865–1873. https://doi.org/10.1016/j.bmcl.2019.05.042.
[12] A. Massarotti, A. Coluccia, R. Silvestri, G. Sorba, A. Brancale, The tubulin colchicine domain: A molecular modeling perspective, ChemMedChem. 7 (2012) 33–42. https://doi.org/10.1002/cmdc.201100361.
[13] Y. Lu, J. Chen, M. Xiao, W. Li, D.D. Miller, An overview of tubulin inhibitors that interact with the colchicine binding site, Pharm. Res. 29 (2012) 2943–2971. https://doi.org/10.1007/s11095-012-0828-z.
[14] A.M. Tsimberidou, W. Akerley, M.C. Schabel, D.S. Hong, C. Uehara, A. Chhabra, T. Warren, G.G. Mather, B.A. Evans, D.P. Woodland, E.A. Swabb, R. Kurzrock, Phase I clinical trial of MPC-6827 (Azixa), a microtubule destabilizing agent, in patients with advanced cancer, Mol. Cancer Ther. 9 (2010) 3410–3419. https://doi.org/10.1158/1535-7163.MCT-10-0516.
[15] J.Y. Bruce, J. Eickhoff, R. Pili, T. Logan, M. Carducci, J. Arnott, A. Treston, G. Wilding, G. Liu, A phase II study of 2-methoxyestradiol nanocrystal colloidal dispersion alone and in combination with sunitinib malate in patients with metastatic renal cell carcinoma progressing on sunitinib malate, Invest. New Drugs. 30 (2012) 794–802. https://doi.org/10.1007/s10637-010-9618-9.
[16] P. Liu, Y. Qin, L. Wu, S. Yang, N. Li, H. Wang, H. Xu, K. Sun, S. Zhang, X. Han, Y. Sun, Y. Shi, A phase i clinical trial assessing the safety and tolerability of combretastatin A4 phosphate injections, Anticancer. Drugs. 25 (2014) 462–471. https://doi.org/10.1097/CAD.0000000000000070.
[17] D.M. Patterson, M. Zweifel, M.R. Middleton, P.M. Price, L.K. Folkes, M.R.L. Stratford, P. Ross, S. Halford, J. Peters, J. Balkissoon, D.J. Chaplin, A.R. Padhani, G.J.S. Rustin, Phase I clinical and pharmacokinetic evaluation of the vascular-disrupting agent OXi4503 in patients with advanced solid tumors, Clin. Cancer Res. 18 (2012) 1415–1425. https://doi.org/10.1158/1078-0432.CCR-11-2414.
[18] P. Sanna, A. Carta, L. Gherardini, Synthesis and antimycobacterial activity of 3-aryl- , 3-cyclohexyl- and 3-heteroaryl-, 57 (2002) 79–87.
[19] A. Carta, P. Sanna, M. Palomba, L. Vargiu, M. La Colla, R. Loddo, Synthesis and antiproliferative activity of 3-aryl-2-(1H-benzotriazol-1-yl)acrylonitriles. Part III, Eur. J. Med. Chem. 37 (2003) 891–900. https://doi.org/10.1016/S0223-5234(02)01411-3.
[20] A. Carta, M. Palomba, G. Boatto, B. Busonera, M. Murreddu, R. Loddo, Synthesis and antiproliferative activity of 3-aryl-2-[1H(2H)-benzotriazol- 1(2)-yl]acrylonitriles variously

substituted: Part 4, Farmaco. 59 (2004) 637–644. https://doi.org/10.1016/j.farmac.2004.03.004.
[21] A. Carta, I. Briguglio, S. Piras, G. Boatto, P. La Colla, R. Loddo, M. Tolomeo, S. Grimaudo, A. Di Cristina, R.M. Pipitone, E. Laurini, M.S. Paneni, P. Posocco, M. Fermeglia, S. Pricl, 3-Aryl-2-[1H-benzotriazol-1-yl]acrylonitriles: A novel class of potent tubulin inhibitors, Eur. J. Med. Chem. 46 (2011) 4151–4167. https://doi.org/10.1016/j.ejmech.2011.06.018.
[22] I. Briguglio, E. Laurini, M.A. Pirisi, S. Piras, P. Corona, M. Fermeglia, S. Pricl, A. Carta, Triazolopyridinyl-acrylonitrile derivatives as antimicrotubule agents: Synthesis, in vitro and in silico characterization of antiproliferative activity, inhibition of tubulin polymerization and binding thermodynamics, Eur. J. Med. Chem. 141 (2017) 460–472. https://doi.org/10.1016/j.ejmech.2017.09.065.
[23] P. Sanna, A. Carta, M.E.R. Nikookar, Synthesis and antitubercular activity of 3-aryl substituted-2-(1H(2H) benzotriazol-1(2)-yl)acrylonitriles, Eur. J. Med. Chem. 35 (2000) 535–543. https://doi.org/10.1016/S0223-5234(00)00144-6.
[24] H. van de W. and D.K.W. D. A. Smith, Methods and Principles in Medicinal Chemistry, vol. 31: Pharmacokinetics and Metabolism in Drug Design, , Wiley-VCH, Weinheim, 2006.
[25] B.E. Smart, Fluorine substituent effects (on bioactivity), J. Fluor. Chem. 109 (2001) 3–11. https://doi.org/10.1016/S0022-1139(01)00375-X.
[26] S. Purser, P.R. Moore, S. Swallow, V. Gouverneur, Fluorine in medicinal chemistry, Chem. Soc. Rev. 37 (2008) 320–330. https://doi.org/10.1039/b610213c.
[27] O.A.J. Trott, O., AutoDock Vina: Improving the Speed and Accuracy of Docking with a New Scoring Function, Efficient Optimization, and Multithreading, J. Comput. Chem. 31 (2010) 455–461. https://doi.org/10.1002/jcc.21334.
[28] Z. Wang, H. Sun, X. Yao, D. Li, L. Xu, Y. Li, S. Tian, T. Hou, Comprehensive evaluation of ten docking programs on a diverse set of protein-ligand complexes: The prediction accuracy of sampling power and scoring power, Phys. Chem. Chem. Phys. 18 (2016) 12964–12975. https://doi.org/10.1039/c6cp01555g.
[29] H.M. Berman, T. Battistuz, T.N. Bhat, W.F. Bluhm, P.E. Bourne, K. Burkhardt, Z. Feng, G.L. Gilliland, L. Iype, S. Jain, P. Fagan, J. Marvin, D. Padilla, V. Ravichandran, B. Schneider, N. Thanki, H. Weissig, J.D. Westbrook, C. Zardecki, The protein data bank, Acta Crystallogr. Sect. D Biol. Crystallogr. 58 (2002) 899–907. https://doi.org/10.1107/S0907444902003451.
[30] A.J. Morris, G. M., Huey, R., Lindstrom, W., Sanner, M. F., Belew, R. K., Goodsell, D. S. and Olson, AutoDock4 and AutoDockTools4: Automated Docking with Selective Receptor Flexibility, J. Comput. Chem. 16 (2009) 2785–91.
[31] K. Stott, J. Keeler, Q.N. Van, A.J. Shaka, One-Dimensional NOE Experiments Using Pulsed Field Gradients, J. Magn. Reson. 125 (1997) 302–324. https://doi.org/10.1006/jmre.1997.1110.
[32] Y. Binev, M.M.B. Marques, J. Aires-de-Sousa, Prediction of1H NMR coupling constants with associative neural networks trained for chemical shifts, J. Chem. Inf. Model. 47 (2007) 2089–2097. https://doi.org/10.1021/ci700172n.
[33] M. Lai, V. La Rocca, R. Amato, G. Freer, M. Costa, P.G. Spezia, P. Quaranta, G. Lombardo, D. Piomelli, M. Pistello, Ablation of Acid Ceramidase Impairs Autophagy and Mitochondria Activity in Melanoma Cells, Int. J. Mol. Sci. 22 (2021) 3247. https://doi.org/10.3390/ijms22063247.
[34] A. Daina, O. Michielin, V. Zoete, SwissADME: a free web tool to evaluate pharmacokinetics, drug-likeness and medicinal chemistry friendliness of small molecules, Sci. Rep. 7 (2017) 42717. https://doi.org/10.1038/srep42717.
[35] A. Daina, O. Michielin, V. Zoete, iLOGP: A Simple, Robust, and Efficient Description of n -Octanol/Water Partition Coefficient for Drug Design Using the GB/SA Approach, J. Chem. Inf. Model. 54 (2014) 3284–3301. https://doi.org/10.1021/ci500467k.

[36] C.A. Lipinski, F. Lombardo, B.W. Dominy, P.J. Feeney, Experimental and computational approaches to estimate solubility and permeability in drug discovery and development settings, Adv. Drug Deliv. Rev. (2012). https://doi.org/10.1016/j.addr.2012.09.019.
[37] The PyMOL Molecular Graphics System, Version 2.0 Schrödinger, LLC., (n.d.).
[38] Maestro, version 10.2, Schrödinger, LLC, New York, NY, 2015., (n.d.).
[39] L. RA, S. MB, LigPlot+: multiple ligand-protein interaction diagrams for drug discovery, J. Chem. Inf. Model. 51 (2011) 2778–2786.
[40] K. Eskandari, M. Lesani, Does fluorine participate in halogen bonding?, Chem. - A Eur. J. 21 (2015) 4739–4746. https://doi.org/10.1002/chem.201405054.
[41] C.S. See, M. Kitagawa, P.J. Liao, K.H. Lee, J. Wong, S.H. Lee, B.W. Dymock, Discovery of the cancer cell selective dual acting anti-cancer agent (Z)-2-(1H-indol-3-yl)-3-(isoquinolin-5-yl)acrylonitrile (A131), Eur. J. Med. Chem. 156 (2018) 344–367. https://doi.org/10.1016/j.ejmech.2018.07.011.
[42] L. Sanna, R. Piredda, I. Marchesi, V. Bordoni, S.V. Forcales, D.F. Calvisi, L. Bagella, "Verteporfin exhibits anti-proliferative activity in embryonal and alveolar rhabdomyosarcoma cell lines", Chem. Biol. Interact. 312 (2019) 108813. https://doi.org/10.1016/j.cbi.2019.108813.
[43] J. Barretina, G. Caponigro, N. Stransky, K. Venkatesan, A.A. Margolin, S. Kim, C.J. Wilson, J. Lehár, G. V. Kryukov, D. Sonkin, A. Reddy, M. Liu, L. Murray, M.F. Berger, J.E. Monahan, P. Morais, J. Meltzer, A. Korejwa, J. Jané-Valbuena, F.A. Mapa, J. Thibault, E. Bric-Furlong, P. Raman, A. Shipway, I.H. Engels, J. Cheng, G.K. Yu, J. Yu, P. Aspesi, M. De Silva, K. Jagtap, M.D. Jones, L. Wang, C. Hatton, E. Palescandolo, S. Gupta, S. Mahan, C. Sougnez, R.C. Onofrio, T. Liefeld, L. MacConaill, W. Winckler, M. Reich, N. Li, J.P. Mesirov, S.B. Gabriel, G. Getz, K. Ardlie, V. Chan, V.E. Myer, B.L. Weber, J. Porter, M. Warmuth, P. Finan, J.L. Harris, M. Meyerson, T.R. Golub, M.P. Morrissey, W.R. Sellers, R. Schlegel, L.A. Garraway, The Cancer Cell Line Encyclopedia enables predictive modelling of anticancer drug sensitivity, Nature. 483 (2012) 603–607. https://doi.org/10.1038/nature11003.
[44] Y. Wang, H. Zhang, B. Gigant, Y. Yu, Y. Wu, X. Chen, Q. Lai, Z. Yang, Q. Chen, J. Yang, Structures of a diverse set of colchicine binding site inhibitors in complex with tubulin provide a rationale for drug discovery, FEBS J. (2016). https://doi.org/10.1111/febs.13555.
[45] Z. Zhang, C. Wang, L. Ma, X. Jiang, C. Wu, Y. Wang, Y. Jiang, W. Zheng, Y. Yang, Y. Ma, J. Yang, Molecular mechanism of crolibulin in complex with tubulin provides a rationale for drug design, Biochem. Biophys. Res. Commun. (2019). https://doi.org/10.1016/j.bbrc.2019.02.064.
[46] E.R. Caremoli, R. Labianca, Tivantinib: Critical review with a focus on hepatocellular carcinoma, Expert Opin. Investig. Drugs. 23 (2014) 1563–1574. https://doi.org/10.1517/13543784.2014.949339.
[47] Y.K. Kang, K. Muro, M.H. Ryu, H. Yasui, T. Nishina, B.Y. Ryoo, Y. Kamiya, S. Akinaga, N. Boku, A phase II trial of a selective c-Met inhibitor tivantinib (ARQ 197) monotherapy as a second- or third-line therapy in the patients with metastatic gastric cancer, Invest. New Drugs. (2014). https://doi.org/10.1007/s10637-013-0057-2.
[48] J.W. Goldman, I. Laux, F. Chai, R.E. Savage, D. Ferrari, E.G. Garmey, R.G. Just, L.S. Rosen, Phase 1 dose-escalation trial evaluating the combination of the selective MET (mesenchymal-epithelial transition factor) inhibitor tivantinib (ARQ 197) plus erlotinib, Cancer. (2012). https://doi.org/10.1002/cncr.27575.
[49] A. Aoyama, R. Katayama, T. Oh-hara, S. Sato, Y. Okuno, N. Fujita, Tivantinib (ARQ 197) exhibits antitumor activity by directly interacting with tubulin and overcomes ABC transporter-mediated drug resistance, Mol. Cancer Ther. (2014). https://doi.org/10.1158/1535-7163.MCT-14-0462.
[50] M.M. Mita, M.A. Spear, L.K. Yee, A.C. Mita, E.I. Heath, K.P. Papadopoulos, K.C. Federico,